INTRODUCING THE FOUNDATIONS OF A GENERAL FRAMEWORK FOR CLOSED-LOOP CONTROL IN ADDITIVE MANUFACTURING VIA IN SITU MEASUREMENTS AND SEMANTIC ANNOTATIONS

A Dissertation
Presented to
The Academic Faculty

By

Kévin Garanger

In Partial Fulfillment
of the Requirements for the Degree
Master of Science in the
School of Aerospace Engineering

Georgia Institute of Technology

May 2018

INTRODUCING THE FOUNDATIONS OF A GENERAL FRAMEWORK FOR CLOSED-LOOP CONTROL IN ADDITIVE MANUFACTURING VIA IN SITU MEASUREMENTS AND SEMANTIC ANNOTATIONS

Approved by:

Professor Eric Feron, Advisor
School of Aerospace Engineering
Georgia Institute of Technology

Professor Claudio Di Leo
School of Aerospace Engineering
Georgia Institute of Technology

Professor Martha Grover
School of Chemical & Biomolecular Engineering
Georgia Institute of Technology

Professor Julián Rimoli
School of Aerospace Engineering
Georgia Institute of Technology

Date Approved: April 24, 2018

It is Khnum who made the seven Khnums, Builder of Builders who created what exists.

Sauneron, S. (1959-75). Le temple d'Esna [The temple of Esna].

Institut Français d'Archéologie Orientale (Esna V, no. 367, 14-15)

To my late grandfather Jacques Papon.

ACKNOWLEDGEMENTS

I would like to thank my academic advisor, Prof. Eric Feron, for his wise counseling during the elaboration of this thesis. The support, consideration, and independence that he gave me have been of a tremendous help to reach my objectives during my research. I am also grateful to the the members of my committee for the helpful feedback that clarified my ideas and led me to take the direction I chose.

This work could not have been achieved without the help of my fellow graduate student Thanakorn Khamvilai, who was the person responsible for the execution of the experiments described in this thesis. His skills admirably completed mines and I could not emphasize enough the teamwork which is behind the results presented here. I also would like to thank Juan-Pablo Afman for his advice on the experimental setting we used.

In addition, I would like to express my gratitude to Dr. Dan Berrigan for his feedback during the early stage of the project presented in this work.

Last but not least, I would like to thank my parents and my sister for always supporting my choices and giving me the freedom of deciding for myself the path I would follow in my life.

TABLE OF CONTENTS

Acknowledgments v

List of Tables x

List of Figures xi

Chapter 1: A proof of concept: 3D Printing of a leaf spring 1

1.1 Introduction 1

1.2 Additive manufacturing of a leaf spring 2

1.2.1 Process description 2

1.2.2 Experimental setting 4

1.3 Feedback control law 6

1.3.1 Estimating the stiffness of a stack of leaves 6

1.3.2 Estimating the final stiffness 10

1.3.3 Optimal control of the printing process 11

1.3.4 Process noise parameterization 12

1.3.5 Filtering algorithm 13

1.4 Simulation 14

1.4.1 Comparison between simulated closed-loop and open-loop control . 15

1.4.2 Comparison between perfect and imperfect model for simulated closed-loop control 15

1.5 Experiments 18

1.5.1 Determination of the process and observation noises 19

1.5.2 Printing the leaf spring 19

1.6 Conclusion 22

Chapter 2: A second experiment: 3D Printing of a cantilever beam 23

2.1 Introduction 23

2.2 Physics 23

2.3 State estimation 25

2.3.1 Problem dynamics 25

2.3.2 Observation of the process 26

2.3.3 Kalman filter 26

2.4 Control law 27

2.4.1 Minimizing the quantity of used material 27

2.4.2 Minimizing the probability of failure 28

2.4.3 Minimizing the log-likelihood of failure 30

2.5 Determination of the models parameters 31

2.5.1 Printed test specimens 31

2.5.2 Stiffness measurements 31

2.6 Experimental results 35

2.6.1 Experiment description 35

2.6.2 Results 35

2.6.3 Results discussion 36

2.7 Conclusion 36

Chapter 3: Generalizing closed-loop control capabilities to the manufacturing of any part 38

3.1 Formulation of a general control problem 39

3.1.1 Objective definition 39

3.1.2 State space of the system 41

3.1.3 Control space of the system 41

3.1.4 Dynamics of the system 42

3.2 State estimation and process monitoring 43

3.2.1 Nondestructive testing 43

3.2.2 Relations between NDT measurements and manufactured object state 44

3.3 Semantic annotations of 3D printing files 45

3.3.1 Existing 3D printing file formats 48

3.3.2 Formal definition of AM files properties 49

3.4 From semantic annotations to feedback control laws: Closing the loop based on the represented properties at the file level 52

3.4.1 Online topology optimization 53

Chapter 4: Conclusion 56

Appendix A: Tables for chapter 1 59

Appendix B: Tables for chapter 2 61

References 69

LIST OF TABLES

1.1 Measured stiffness (kg/mm) at steps $1, 2, 3$ using the filtering algorithm and the two baselines with the absolute error in the stiffness at each final step . . 21

A.1 Mean of the stiffness of each specimen from 5 measurements (kg/mm) . . . 59

A.2 Standard deviation of the stiffness of each specimen from 5 measurements (kg/mm) 60

A.3 Mean and standard deviation of the stiffness of specimens of equal density (kg/mm) 60

A.4 % Printed infill density of the specimen at steps $1, 2, 3$ using the filtering algorithm and the two baselines obtained from equation (1.9) 60

B.1 Stiffness measurement at each control step in g/mm (closed-loop) and input width of each stack of 50 layers in mm in the closed-loop and open-loop cases 62

B.2 Stiffness measurements in g/mm of the three completed specimens printed with open-loop control 62

B.3 Stiffness measurements in g/mm of the completed specimen printed with closed-loop control 62

B.4 Percentage of deviation of the final compliance with the target for each specimen 62

LIST OF FIGURES

1 Integrated 3D printing process xv

1.1 Picture of a leaf spring of a Willys M38 [31] 3

1.2 Stack of 3 leaves with a load applied on top and 4 supports on the bottom corners for measuring stiffness 3

1.3 Printrbot Simple 3D printer - 1405 Model 4

1.4 Example specimens with different percentages of infill density 5

1.5 The setup of the 3-point bending test 5

1.6 Plot between an applied load and a vertical deflection of a single specimen with 10% infill density from 5 measurements. Each color represents a measurement made of several data points represented by $\star$. Lines represent the linear regressions of these data points. 6

1.7 The process block-diagram 13

1.8 Distribution of the final stiffness (in kg/mm) after 1000 process simulations of an open-loop and closed-loop control 15

1.9 Distribution of the final stiffness (in kg/mm) after 1000 process simulations of a closed-loop control with increased noise 16

1.10 Distribution of the final stiffness (in kg/mm) after 1000 process simulations of a closed-loop control with bias in observations and process 16

1.11 Distribution of the final stiffness (in kg/mm) after 1000 process simulations of a closed-loop and open-loop controls with altered model parameter α . . 17

1.12 Distribution of the final stiffness (in kg/mm) after 1000 process simulations of a closed-loop control with process following a Gamma distribution . . . 18

1.13 Stiffness measurements for 15 specimens of different infill densities. $\circ$ represents each measurement. Δ represents the average stiffness of each specimen from 5 measurements. $\oplus$ represents the average stiffness of specimens with the same infill density. R, G, and B represent the $1^{st}, 2^{nd}$, and 3^{rd} specimen of the same infill density, respectively. The line represents the linear regression of $\oplus$ data given by equation (1.10). 20

1.14 Stiffness measurements at steps $1, 2, 3$ for $n = 3, K = 30$. $\circ$ represents a measurement. Red is used for closed-loop with filtering. Blue is used for closed-loop without filtering. Dashed **black** is used for open-loop. Green marked coordinates represent the desired values of stiffness. 21

1.15 Stiffness measurements at steps $1, 2, 3$ for $n = 3, K = 40$. Legend is same as in Figure 1.14 22

2.1 Example of a 3D printed cantilever beam 24

2.2 4 specimens of different widths 32

2.3 Measurement of the stiffness of a full specimen printed with open-loop control 33

2.4 Deflection and load measurements on test specimens 34

2.5 Interpolation between stiffness and width of the test specimens 34

3.1 Workflow of a typical AM process 46

3.2 Excerpt of an STL file describing a cube 48

3.3 Example of a 3D tetrahedral mesh of a cube generated from an STL file with tetgen 51

SUMMARY

During the last decade, additive manufacturing (AM) has become increasingly popular for rapid prototyping, but has remained relatively marginal beyond the scope of prototyping when it comes to applications with tight tolerance specifications, such as in aerospace. Despite a strong desire to supplant many aerospace structures with printed builds, additive manufacturing has largely remained limited to prototyping, tooling, fixtures, and non-critical components. There are numerous fundamental challenges inherent to additive processing to be addressed before this promise is realized. One ubiquitous challenge across all AM motifs is to develop processing-property relationships through precise, in situ monitoring coupled with formal methods and feedback control.

Today, feedback control is, in general, a well-accepted discipline whose impact on the proper operation of complex systems can be beneficial. In some instances, systems could not operate without feedback control: Such is the case of nuclear plants and advanced fighter aircraft [24]. To improve the quality of AM produced builds, it is now commonly recognized that one of the next steps is to create closed-loop and adaptive control systems with feedback control capabilities [12, 25, 38]. Specific cases of closed-loop and adaptive controls for AM have been developed. For instance, adaptive and closed-loop control systems have been implemented in gas metal arc welding (GMAW) and powder bed fusion processes to control the deposition height based on a vision sensor [76, 77] and to control the deposition temperature of the Ti-6Al-4V alloy by altering the tool paths. While these demonstrations are the first steps towards real-time feedback and control, they are unable to account for varying materials properties or deviations from intended specifications. The geometric and performance based object specifications that are to be defined by this work form the foundational sets of targets and constraints that are used in classical control theory.

The objective of this thesis is to lay the foundations of a framework for closed-loop control in additive manufacturing. An examination of the process leading to the construc-

tion of an object in AM, from its computer aided design to its actual manufacturing and post-processing, shows that such framework is only possible if it is associated with the files describing such an object. Indeed, AM entails many different manufacturings technologies that rely on significantly different physical processes. Therefore, inventing a framework to formulate any manufacturing process as a control problem might seem an impossible task. In face of that multitude of processes, a way to cut the Gordian knot could be to include all the information necessary to formulate a control problem at the level of the 3D printing files, and to let the different manufacturers use their own control laws to satisfy the requirements expressed in these files. Few 3D printing file formats exist compared to the number of AM technologies. The main one is STL, and there is a global consensus that a successor to STL has to be adopted. Whatever format this successor is, it will be most likely shared by every manufacturer, regardless of the AM technology considered. And since 3D printing files are agnostic of the AM process involved, they can be used as the conveyor of such a general framework for closed-loop control in additive manufacturing.

A significant suggested component of this vision is a set of semantic layers within AM files relevant to the desired material specifications. This semantic layer provides the link between the high-level specifications of the part and the low-level properties driving the feedback laws of the control system, which then evaluates the component during processing and intelligently evolves the build parameters within boundaries defined by semantic specifications. This evaluation and correction loop requires on-the-fly coupling of finite element analysis and topology optimization. The required parameters for this analysis are all extracted from the semantic layer and can be modified in situ to satisfy the global specifications. Therefore, the representation of what is printed changes during the printing process to compensate for eventual imprecision or drift arising during the manufacturing process. The whole process of intelligent additive manufacturing is described in Fig. 1.

The goal of this thesis is to justify the relevance of closed-loop control in AM, and to pave the way for the creation of a general framework to formulate AM processes as control

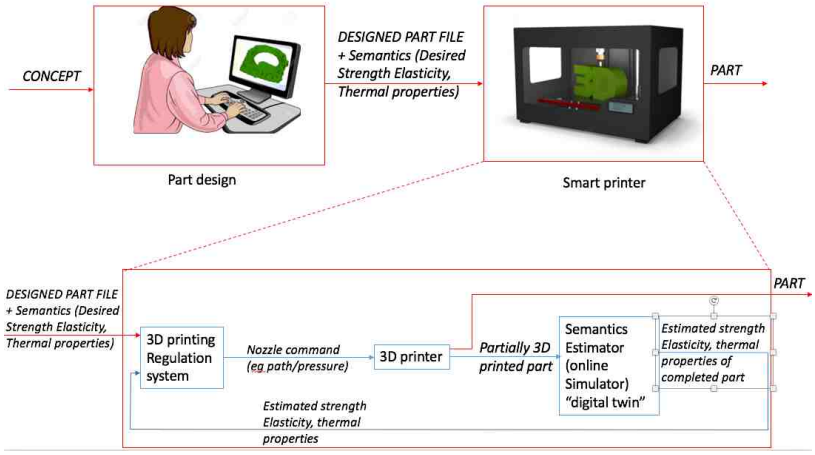

Figure 1: Integrated 3D printing process

problems where feedback can be widely adopted. Section 1 of this thesis presents an experiment performed at the end of 2017 that shows the relevance of feedback control in AM. Section 2 describes a second experiment, more elaborated, that was performed in 2018 and that differs from the first one by considering measurements that were truly performed in situ while pausing the printing process. Finally, section 3 presents the generalization of closed-loop control in AM by presenting the concept of semantics for AM files by introducing the idea of adapting the build local parameters through topology optimization.

CHAPTER 1

A PROOF OF CONCEPT: 3D PRINTING OF A LEAF SPRING

1.1 Introduction

This chapter presents the integration of a feedback control loop during the printing of a plastic object using Fused Deposition Modeling (FDM), as specific process of additive manufacturing. The printed object is a leaf spring made of several parts of different infill density values, which are the control variables in this problem. In order to achieve a desired objective stiffness, intermediate stiffness measurements are taken after each part is completed and the infill density is adjusted accordingly in a closed-loop framework. Objects printed with AM often use porous structures with different possible patterns because of the good mechanical properties and the gain of weight obtained by those structures [16, 55, 75]. The density of such a pattern is the control variable modified throughout this experiment. The dynamics of the system are not based on a physical model relating the input (the infill density) with the output (the stiffness of the printed object), but are based on a purely statistical model. Preliminary measurements were performed on test specimens to show that such a model can be used, and to determine the parameters of this model. The absolute error in the stiffness at the end of printing is reduced from 11.63% to 1.34% by using a closed-loop instead of an open-loop control. This experiments serves as a proof of concept to show the relevance of using feedback control in additive manufacturing. By considering the printing process and the measurements as stochastic processes, we show how stochastic optimal control and Kalman filtering can be used to improve the quality of objects manufactured with rudimentary printers. First the setting of the experiment performed is described in details in section 1.2. Then, from a basic probabilistic model relating the input and output of our system, an optimal control law is derived in section 1.3. From this model, simulations

are performed to assess its performance in section 1.4. Finally, in section 1.5, the results of the experiment are given along with some concluding remarks in section 1.6.

1.2 Additive manufacturing of a leaf spring

1.2.1 Process description

This experiment consists in the additive manufacturing of a leaf spring. Leaf springs are springs made of several stacked leaves that are commonly used for the suspensions of wheeled vehicles [35] (Figure 1.1). Because a leaf spring is made of several parts built independently and then assembled, its manufacturing is a sequential problem that fits perfectly the framework of a discrete dynamic programming problem. Each step corresponds to the printing of a new leaf and the applied control is chosen to reach a final objective. In this case, a stack of n leaves is designed to have a fixed final geometry and a specific stiffness along the vertical axis (Figure 1.2). The stiffness of a leaf is defined a the linear coefficient relating deflection to load applied during a 3-point bending test, assuming a linear relationship. Each leaf is made of the same number of layers and of the same material. Leaves are assumed to be Euler-Bernoulli beams [30] and a 3-point bending test is used to measure their stiffness. In order to achieve the desired stiffness objective, the infill density of each new leaf is adapted in a closed-loop setting. To do so, measurements are performed after the printing of each leaf to evaluate the stiffness of the partially built object and to meet a target overall stiffness. Because the different leaves of the leaf spring are not stuck together, the stiffness of a stack of leaves is approximated as additive in the Euler-Bernoulli theory. Leaves are printed independently before stacking them to ensure that this condition is respected. The additivity property of the stiffness allows the use of a linear Kalman filter to estimate the stiffness at each step more precisely. The derivation of the filtering that is used is detailed in section 1.3 while the parameters of the filters are estimated with some preliminary measurements. The results of those measurements are given in section 1.5.

Figure 1.1: Picture of a leaf spring of a Willys M38 [31]

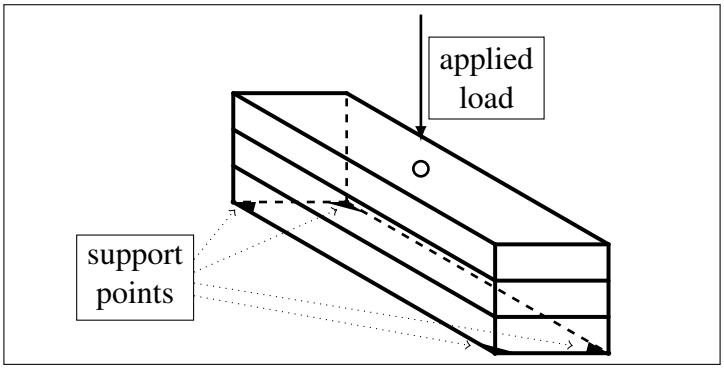

Figure 1.2: Stack of 3 leaves with a load applied on top and 4 supports on the bottom corners for measuring stiffness

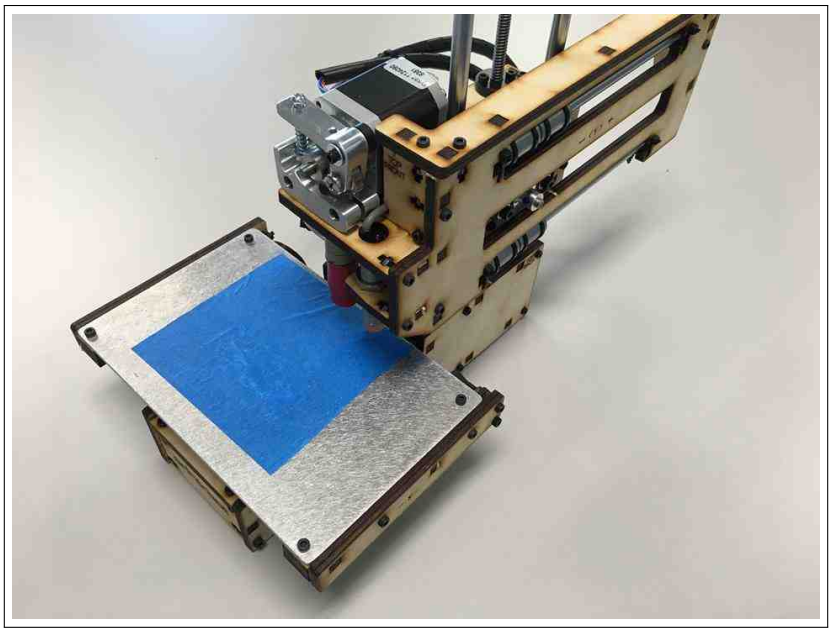

Figure 1.3: Printrbot Simple 3D printer - 1405 Model

1.2.2 Experimental setting

Printing procedure

For this experiment, a low-cost printer was chosen since the objective of this work is proving that feedback control based on in situ measurements can be used to print more reliably with material subject to a high process noise. The Printrbot Simple 3D printer - 1405 Model [56] (Figure 1.3) is chosen because more random variation is expected during the printing process from such a printer than with a high-performance one [59]. The filament type used in this experiment is Polylactic Acid (PLA), which is provided with the printer package. The identical Computer-Aided-Design (CAD) model of every specimen is developed using Solidworks [18]. The G-Code [26] files are generated using the default setting of Cura [73], except for the percentage of infill density. Finally, Pronterface [79] is used as a graphic user interface (GUI) for monitoring and communicating between the 3D printer and a computer. Some example specimens with different percentages of infill density are showed in Figure 1.4.

(a) 10% infill density (b) 20% infill density (c) 30% infill density

Figure 1.4: Example specimens with different percentages of infill density

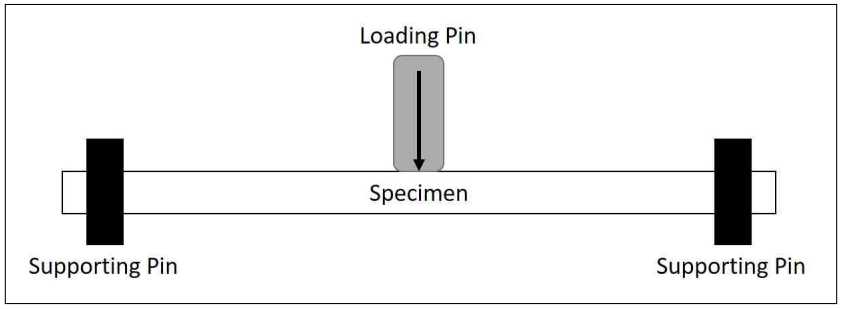

Figure 1.5: The setup of the 3-point bending test

Stiffness measurement procedure

In this experiment, the preparation of the PLA specimens and of the three-point bending test (Figure 1.5) is performed based on ASTM D790 [3], which is the standard testing method for flexural properties of plastic materials. Since each specimen is required to be stacked over the next one, we constrained our experiment within the elastic region of the material. Then a load acting on the specimen and its vertical deflection were measured at each time step. After that, the stiffness is determined from the slope of the linear regression between the deflection and load data sets (Figure 1.6). Note that in this figure, some geometric nonlinearities can be observed, suggesting that the tests performed were not restricted to the domain of elasticity of the specimens. A better model would require more careful measurements. However, the objective of this not work is not exactly to derive a precise model but rather to show that closed-loop control can be useful without a perfect model.

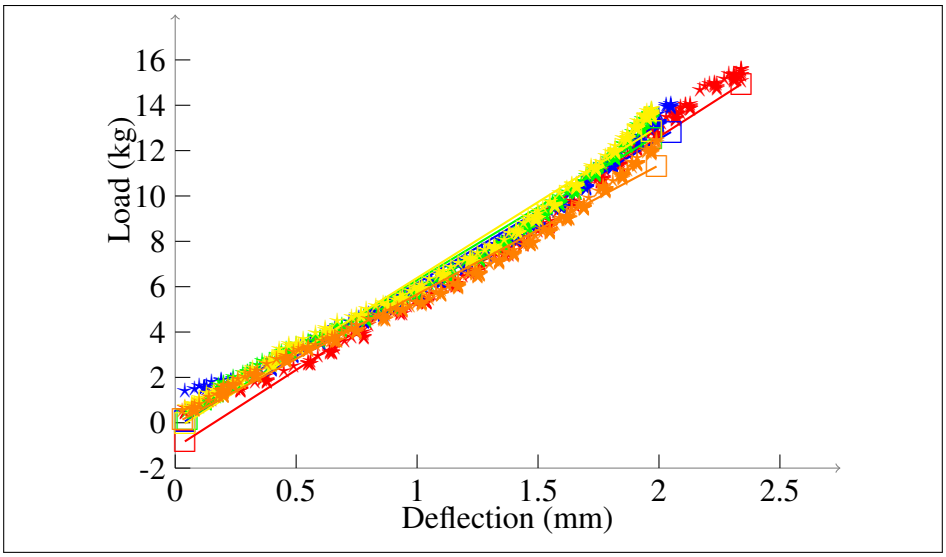

Figure 1.6: Plot between an applied load and a vertical deflection of a single specimen with 10% infill density from 5 measurements. Each color represents a measurement made of several data points represented by $\star$. Lines represent the linear regressions of these data points.

1.3 Feedback control law

In this section, an optimal control law that aims at reaching a target stiffness while minimizing a specified cost function is derived. At each step i, a new measurement of the stiffness is performed and taken into account to refine the estimate of the predicted stiffness at the final step n. This is done by using filtering to estimate the actual stiffness of a stack of leaves. Two types of noises are considered: a process noise that comes from the inaccuracy of the printer and from the changing environment, and a measurement noise. Both are assumed to follow independent normal laws. In the following subsections the process to estimate the stiffness of a stack at each step is described. Then this stiffness estimate is used to obtain an optimal control law. The chosen parameterization of the process noise is also detailed while the algorithm obtained from the optimal control law is described.

1.3.1 Estimating the stiffness of a stack of leaves

In this subsection the stiffness of a stack of printed leaves is estimated given the controls that have been previously applied and given the measurements after each new printed leaf.

This is equivalent to applying a linear Kalman filter. For a sequence of controls $(d_i)_{i\leq n}$, let K_i be the stiffness of the first i printed leaves stacked together. This is a random variable defined recursively by

$$K_0 = 0$$

and

$$K_{i+1} = K_i + \mu_p(d_{i+1}) + \epsilon_{i+1} \tag{1.1}$$

where

$$\epsilon_i \sim \mathcal{N}(0, \sigma_p)$$

and

$$\mu_p(d_i)$$

are respectively independent identically distributed random variables and the mean stiffness of a single leaf of density d_i.

The stiffness observations of a stack of the first i leaves are also defined by

$$\bar{K}_i = K_i + \bar{\epsilon}_i \tag{1.2}$$

where

$$\bar{\epsilon}_i \sim \mathcal{N}(0, \sigma_o)$$

are independent identically distributed random variables independent of each process noise $(\epsilon_j)_{j\leq n}$, previous stiffnesses observations $(\bar{K}_j)_{j<i}$, and past controls $(d_j)_{j\leq i}$.

To derive the probability law of the stiffness K_i given the previous observations and

past controls, the Bayes rule is applied to the joint probability of K_i and $\bar{K}_i$.

$$
\begin{aligned}
& p(K_i|(\bar{K}_j)_{j\leq i},(d_j)_{j\leq i})p(\bar{K}_i|(\bar{K}_j)_{j<i},(d_j)_{j\leq i}) \\
&= p(K_i,\bar{K}_i|(\bar{K}_j)_{j<i},(d_j)_{j\leq i}) \\
&= p(\bar{K}_i|K_i,(\bar{K}_j)_{j<i},(d_j)_{j\leq i})p(K_i|(\bar{K}_j)_{j<i},(d_j)_{j\leq i})
\end{aligned}
$$

Since the stiffness observations are independent, it yields

$$
\begin{aligned}
& p(K_i|(\bar{K}_j)_{j\leq i},(d_j)_{j\leq i})p(\bar{K}_i|(\bar{K}_j)_{j<i},(d_j)_{j\leq i}) \\
&= p(\bar{K}_i|K_i)p(K_i|(\bar{K}_j)_{j<i},(d_j)_{j\leq i})
\end{aligned} \tag{1.3}
$$

With the observation relation (1.2), the probability distribution of the observation is given by

$$
p(\bar{K}_i|K_i) = \frac{1}{\sqrt{2\pi\sigma_o^2}}\exp\left(-\frac{1}{2}\frac{(\bar{K}_i-K_i)^2}{\sigma_o^2}\right)
$$

Then, using the process relation (1.1),

$$
\begin{aligned}
& p(K_i|(\bar{K}_j)_{j<i},(d_j)_{j\leq i}) \\
&= \int_{K_{i-1}} p(K_i|K_{i-1},d_i)p(K_{i-1}|(\bar{K}_j)_{j<i},(d_j)_{j\leq i})\mathrm{d}K_{i-1} \\
&= \int_{K_{i-1}} \frac{1}{\sqrt{2\pi\sigma_p^2}}\exp\left(-\frac{1}{2}\frac{(K_i-K_{i-1}-\mu_p(d_i))^2}{\sigma_p^2}\right) \\
&\quad \times p(K_{i-1}|(\bar{K}_j)_{j<i},(d_j)_{j<i})\mathrm{d}K_{i-1}
\end{aligned} \tag{1.4}
$$

Reusing equation (1.2) leads to

$$
\begin{aligned}
& p(\bar{K}_i|(\bar{K}_j)_{j<i},(d_j)_{j\leq i}) \\
&= \int_{K_i} p(\bar{K}_i|K_i)p(K_i|(\bar{K}_j)_{j<i},(d_j)_{j\leq i})\mathrm{d}K_i \\
&= \int_{K_i} \frac{1}{\sqrt{2\pi\sigma_o^2}}\exp\left(-\frac{1}{2}\frac{(\bar{K}_i-K_i)^2}{\sigma_o^2}\right) \\
&\quad \times p(K_i|(\bar{K}_j)_{j<i},(d_j)_{j\leq i})\mathrm{d}K_i
\end{aligned} \tag{1.5}
$$

Therefore ,these three equations give a recursive relation for the derivation of $p(K_i|(\bar{K}_j)_{j\leq i},(d_j)_{j\leq i})$.

Assuming that $p(K_{i-1}|(\bar{K}_j)_{j<i},(d_j)_{j<i})$ is the probability of a normal law of mean μ_{i-1} and variance σ_{i-1}, replacing in equation (1.4) gives

$$
\begin{aligned}
& p(K_i|(\bar{K}_j)_{j<i},(d_j)_{j\leq i}) \\
&= \frac{1}{\sqrt{2\pi(\sigma_p^2+\sigma_{i-1}^2)}}\exp\left(-\frac{1}{2}\frac{(K_i-\mu_{i-1}-\mu_p(d_i))^2}{\sigma_p^2+\sigma_{i-1}^2}\right)
\end{aligned}
$$

Then, replacing in equation (1.5),

$$
\begin{aligned}
& p(\bar{K}_i|(\bar{K}_j)_{j<i},(d_j)_{j\leq i}) \\
&= \frac{1}{\sqrt{2\pi(\sigma_o^2+\sigma_p^2+\sigma_{i-1}^2)}}\exp\left(-\frac{1}{2}\frac{(\bar{K}_i-\mu_{i-1}-\mu_p(d_i))^2}{\sigma_o^2+\sigma_p^2+\sigma_{i-1}^2}\right)
\end{aligned}
$$

These two results are plugged into the observation law in equation (1.3), which gives

$$
\begin{aligned}
& p(K_i|(\bar{K}_j)_{j\leq i},(d_j)_{j\leq i}) \\
&= \frac{1}{\sqrt{2\pi\sigma_i^2}}\exp\left(-\frac{1}{2}\frac{(K_i-\mu_i)^2}{\sigma_i^2}\right)
\end{aligned}
$$

With

$$\mu_i = \frac{\bar{K}_i(\sigma_p^2 + \sigma_{i-1}^2) + (\mu_{i-1} + \mu_p(d_i))\sigma_o^2}{\sigma_o^2 + \sigma_p^2 + \sigma_{i-1}^2} \tag{1.6}$$

and

$$\sigma_i^2 = \frac{\sigma_o^2(\sigma_p^2 + \sigma_{i-1}^2)}{\sigma_o^2 + \sigma_p^2 + \sigma_{i-1}^2} \tag{1.7}$$

By initializing with $\mu_0 = 0$ and $\sigma_0 = 0$, it is easy to verify that the conditional probability of K_1 given $\bar{K}_1$ and d_1 indeed follows a normal law with parameters given by equations (1.6) and (1.7) with $i = 1$. An induction argument proves that those relations are true for every $i \geq 1$.

Remark 1 *Equation (1.7) defines a Riccati difference equation. It can be solved to provide an expression of σ_i^2 independent of σ_{i-1}^2.*

Remark 2 *The process noise variance σ_p^2 is assumed to be a constant variable but the results would be unchanged if it depended on the control d_i.*

Remark 3 *The observation noise variance σ_o^2 can be reduced by taking several measurements of the same stack. In that case in equation (1.7) the observation noise variance will simply be divided by the number of observations.*

1.3.2 Estimating the final stiffness

Let μ_i be the stiffness of the first i stacked leaves taken altogether. Given the next controls $(d_j)_{i<j\leq n}$ too, the final stiffness K_n of the stacked n leaves can be estimated by:

$$\mathbb{E}(K_n|(\bar{K}_j)_{1\leq j\leq i}, (d_j)_{1\leq j\leq n}) = \mu_i + \sum_{j=i+1}^{n} \mu_p(d_j)$$

1.3.3 Optimal control of the printing process

In this section, are derived the controls $(d_j)_{j\leq n}$ to minimize the expectation of a cost function $J(d_1,\dots,d_n,K_1,\dots,K_n)$ while reaching the objective stiffness K.

At step i, let $(d_j^*)_{j\leq i}$ be the chosen values at the previous steps. Let $\mathcal{H}_i$ be the set of real-valued $(d_j)_{i<j\leq n}$ verifying the equation

$$\sum_{j=i+1}^{n} \mu_p(d_j) = K - \mu_i$$

With this definition, the next controls are $n-i$ values $(d_j^i)_{i<j\leq n}$ such that

$$\begin{aligned}
&\mathbb{E}\big(J(d_1^*,\dots,d_i^*,d_{i+1}^i,\dots,d_n^i,K_1,\dots,K_n) \\
&\qquad\qquad |(\bar{K}_j)_{1\leq j\leq i},(d_j^*)_{1\leq j\leq i},(d_j^i)_{i<j\leq n}\big) \\
&= \min_{(d_j)\in\mathcal{H}_i} \mathbb{E}\big(J(d_1^*,\dots,d_i^*,d_{i+1},\dots,d_n,K_1,\dots,K_n) \\
&\qquad\qquad |(\bar{K}_j)_{1\leq j\leq i},(d_j^*)_{1\leq j\leq i},(d_j)_{i<j\leq n}\big)
\end{aligned}$$

And then the control d_{i+1}^i is applied, such that $d_{i+1}^* := d_{i+1}^i$.

In the following subsection two examples of cost functions are given.

Minimizing the quantity of used material

A possible cost function characterizes the quantity of used printing material:

$$J = \sum_{j=1}^{n} d_j$$

However because the relationship between density and stiffness is linear, the cost function has same value everywhere on $\mathcal{H}_i$, leading to infinitely many possibilities. Instead, the sum

of the squares of the densities can be used:

$$J = \sum_{j=1}^{n} d_j^2$$

In that case, because of the symmetric roles of the different remaining leaves in the cost function and in the constraints, all $(d_j^i)_{i<j\leq n}$ are equal and

$$\mu_p(d_j^i) = \frac{1}{n-i}(K - \mu_i), \forall j, i < j \leq n \tag{1.8}$$

This is the cost function that is used in the rest of the experiment.

1.3.4 Process noise parameterization

In the experiments performed in the next section, the mean stiffness is assumed to be affine in d and the process variance is assumed to be constant.

$$\mu_p(d) = \alpha d + \beta$$

and

$$\sigma_p(d) = \sigma_p > 0$$

These assumptions are based on previous performed measurements on different leaf specimens. Results of these measurements are detailed in section 1.5.

With these assumptions, at each step the optimal control is given by

$$d_{i+1}^* = \frac{K - \mu_i}{\alpha(n-i)} - \frac{\beta}{\alpha}, \forall k, i < k \leq n \tag{1.9}$$

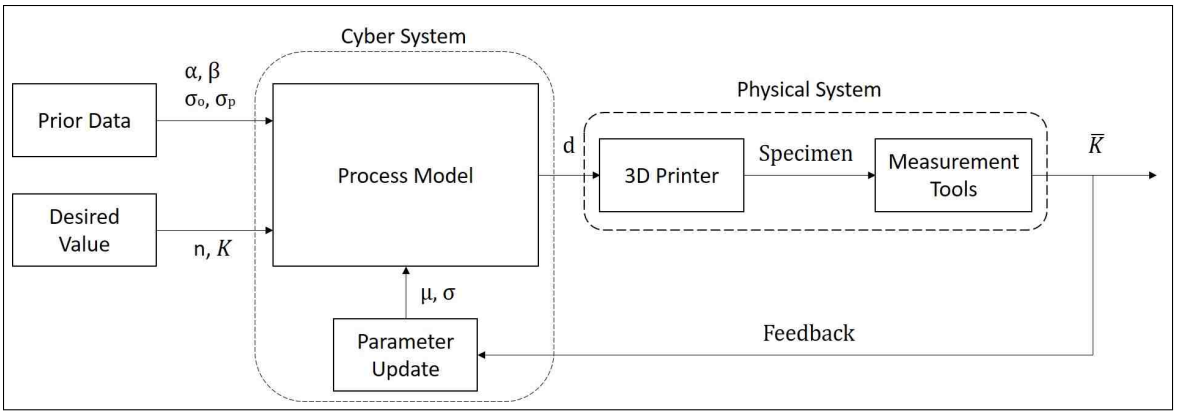

Figure 1.7: The process block-diagram

1.3.5 Filtering algorithm

The derivation of an optimal input density at each step based on an estimate of the stiffness using filtering is the basis of algorithm 1.

Algorithm 1 Optimal printing algorithm with filtering

Require: $n, K, \alpha, \beta, \sigma_p, \sigma_o$

Initialization:

$\mu = 0$

$\sigma^2 = 0$

Printing:

for $i = 0$ to $n - 1$ **do**

  $d := \frac{K-\mu}{\alpha(n-i)} - \frac{\beta}{\alpha}$

  Print a leaf with input density d

  Measure stiffness of the printed leaves $\bar{K}$

  Update $\mu := \frac{\bar{K}(\sigma_p^2+\sigma^2)+(\mu+\mu_p(d_i))\sigma_o^2}{\sigma_o^2+\sigma_p^2+\sigma^2}$

  Update $\sigma^2 := \frac{\sigma_o^2(\sigma_p^2+\sigma^2)}{\sigma_o^2+\sigma_p^2+\sigma^2}$

end for

Besides specifying the number of stacks n and the desired stiffness K, algorithm 1 requires the knowledge of the density-stiffness affine model parameters α and β, the process

noise standard deviation σ_p, and the observation noise standard deviation σ_o, which all can be obtained from the prior measurement data.

After initialization, there are two essential steps during the printing. The first one is picking an optimal infill density d_i^* for the leaf to print in line 4 based on the estimate of the stiffness and on the density-stiffness model. This step is the control determination step.

The second step which is the measurement update of line 7 and 8, updates the intermediate parameters μ and σ with the measured stiffness $\bar{K}$.

The process of this algorithm is summarized by the block-diagram in Figure 1.7.

1.4 Simulation

In this section, simulations were performed using the statistical model that is described in the previous. These simulations compared the behavior of the closed-loop control algorithm with the open-loop algorithm. Simulation with an erroneous model were also performed. That is, the parameters of the model used to simulate the process were altered from the ones used to determine the controls.

In all the simulations, the parameters used for the update of the Kalman filter and for the control determination are the following:

$$\alpha = 0.5 \text{ kg/mm}^2$$

$$\beta = 5 \text{ kg/mm}$$

$$\sigma_p = 1 \text{ kg/mm}$$

$$\sigma_o = 0.5 \text{ kg/mm}$$

When those parameters are changed in the simulations described below, it means that the the simulation (or sampling of the real stiffness and observation) use different parameters, whereas the update rule and control rely on the unchanged parameters. The chosen target was $K = 100$ kg/mm and the number of leaves $n = 10$. In each figure representing the

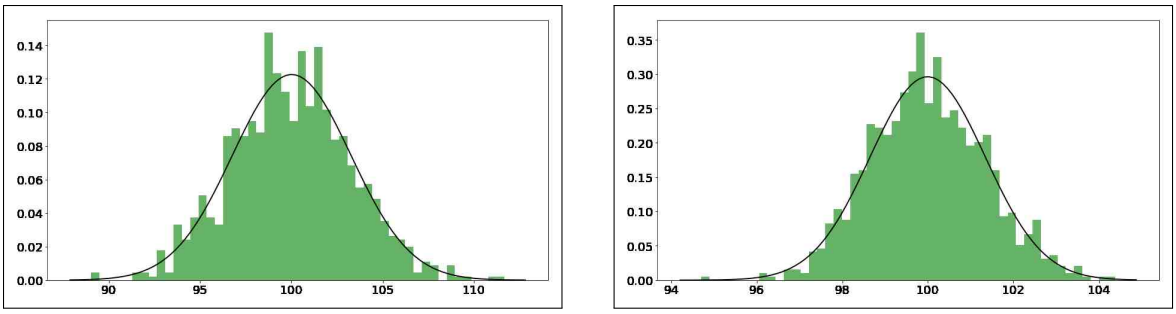

(a) Open-loop control

(b) Closed-loop control

Figure 1.8: Distribution of the final stiffness (in kg/mm) after 1000 process simulations of an open-loop and closed-loop control

repartition of the simulation results, a normal distribution was fitted to the sample distribution and plotted.

1.4.1 Comparison between simulated closed-loop and open-loop control

1000 simulations were performed for both the closed-loop and open-loop control. Because the environment used to simulate the process and observations used the same parameters α, β, σ_o and σ, the mean of the reached stiffness is very close to the target in both cases, but a difference in the standard deviation is noticeable. Standard deviation is higher for the open-loop control, as expected. In the closed-loop control case, the mean of the final stiffness over all the simulations was 100.042 kg/mm with a standard deviation of 1.308 kg/mm. In the open-loop control case, the mean of the final stiffness over all the simulations was 100.065 kg/mm with a standard deviation of 3.29 kg/mm. The distribution of the final stiffnesses is reported in Figure 1.8.

1.4.2 Comparison between perfect and imperfect model for simulated closed-loop control

In this section, the process and observations were simulated by changing some of the parameters, while the controls and Kalman filter updates used the same parameters are mentioned previously. As shown in Figure 1.9, augmenting the real process noise had more influence than increasing the real observation noise. With the closed-loop control, the final stiffness standard deviation jumped to 2.06 kg/mm when increasing the process noise and

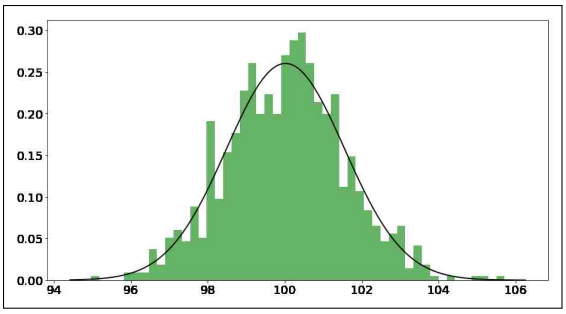

(a) Increased observation noise ($\sigma_o = 3$ kg/mm)

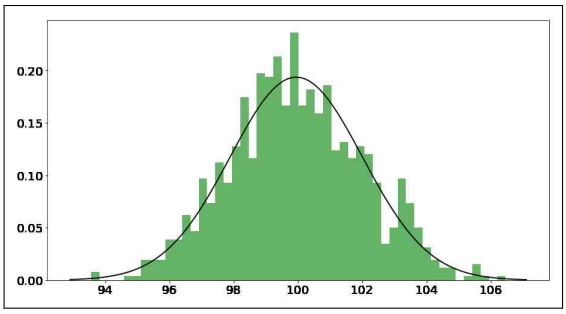

(b) Increased process noise ($\sigma_p = 3$ kg/mm)

Figure 1.9: Distribution of the final stiffness (in kg/mm) after 1000 process simulations of a closed-loop control with increased noise

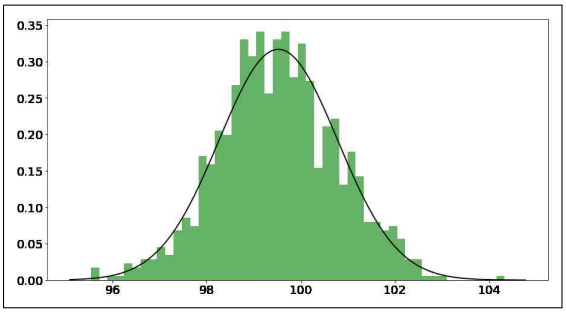

(a) Systematic observation bias (+0.5 kg/mm)

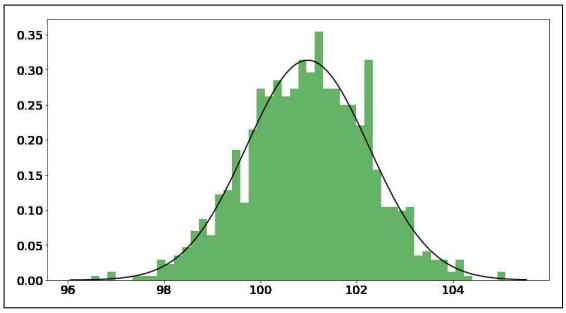

(b) Systematic process bias (+0.5 kg/mm)

Figure 1.10: Distribution of the final stiffness (in kg/mm) after 1000 process simulations of a closed-loop control with bias in observations and process

to 1.545 kg/mm when increasing the observation noise.

A simulation was also performed with a systematic process bias of 0.5 kg/mm. The variance of the final stiffness was not affected (1.272 kg/mm) but the mean was shifted to 100.978 kg/mm, which is still close to the target considering such an important drift. Adding an observation bias of 0.5 kg/mm also didn't affect the variance (1.259 kg/mm) but modified the final mean (99.522 kg/mm). Again, modifying the process noise affected more the final results than modifying the observation noise. Distributions are shown in Figure 1.10.

Simulations were also made by changing α to 0.4 and 0.6 kg/mm^2 with an open-loop and a closed-loop control. With a closed-loop control, lowering α changed the final mean to 97.203 kg/mm while not significantly affecting the final variance (1.354 kg/mm), and increasing α changed the final mean to 101.130 kg/mm and the final variance to 1.267 kg/mm. With an open-loop control, lowering α changed the final mean to 90.106 kg/mm while also

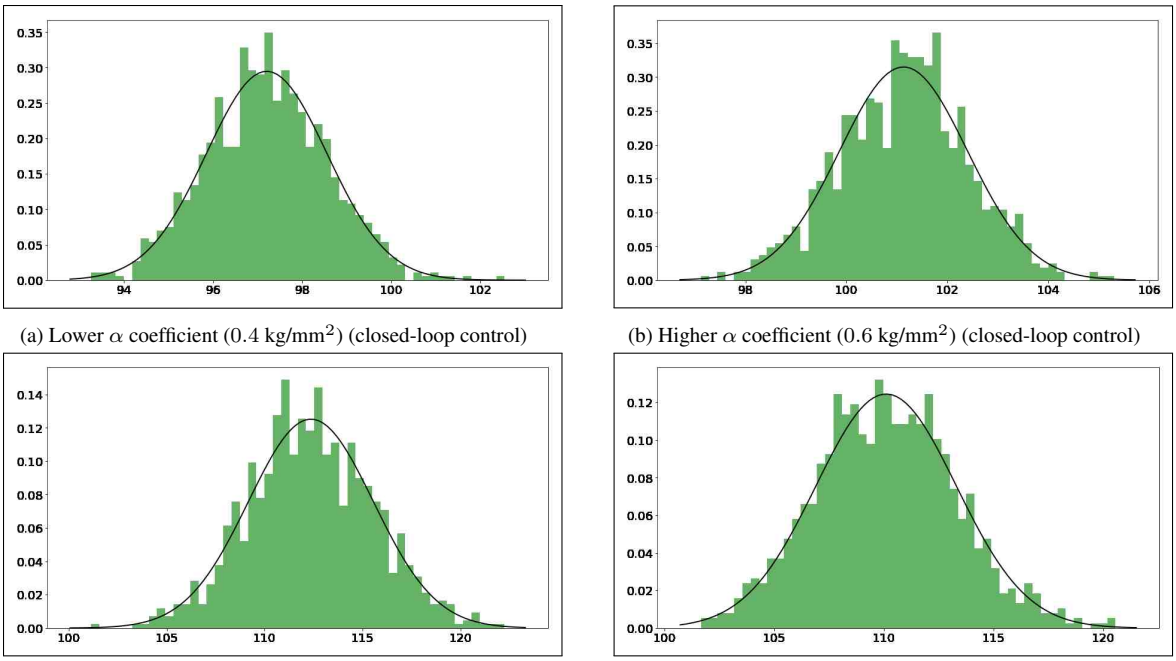

(a) Lower α coefficient (0.4 kg/mm^2) (closed-loop control)

(b) Higher α coefficient (0.6 kg/mm^2) (closed-loop control)

(c) Lower α coefficient (0.4 kg/mm^2) (open-loop control)

(d) Higher α coefficient (0.6 kg/mm^2) (open-loop control)

Figure 1.11: Distribution of the final stiffness (in kg/mm) after 1000 process simulations of a closed-loop and open-loop controls with altered model parameter α

not significantly affecting the final variance (3.065 kg/mm), and increasing α changed the final mean to 110.093 kg/mm and the final variance to 3.204 kg/mm. These results clearly show the advantage of closed-loop control and its robustness to model imprecision. Results are reported in Figure 1.11.

Finally, a last experiment was performed by changing the distribution of the actual process to a Gamma distribution whose mean is equal to the expected stiffness ($\mu_p(d)$ and whose standard deviation is equal to σ_p (1 kg/mm). An advantage of such a distribution is that it is positive, which is more realistic in our setting. The final stiffness mean (100.021) was close to the target and the standard deviation still low (1.278 kg/mm). Therefore the normal distribution hypothesis is good enough to guarantee good results even if the real distribution of the process is not exactly normal. Figure 1.12 shows the distribution of the final stiffnesses in this case.

The different comparisons carried out in this subsection show that even an imprecise model can still lead to a good precision on the final stiffness by using a closed-loop feed-

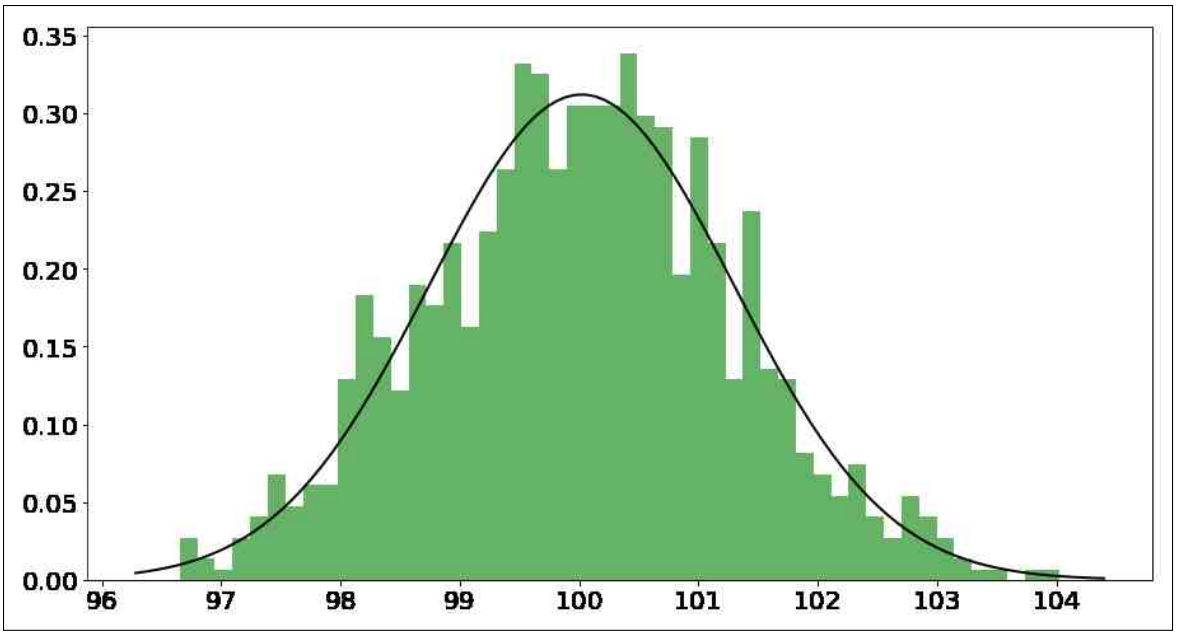

Figure 1.12: Distribution of the final stiffness (in kg/mm) after 1000 process simulations of a closed-loop control with process following a Gamma distribution

back.

1.5 Experiments

In this section, two different sets of experiments are described. The first set of experiments aimed at validating the hypothesis that the process law mean is affine and that the variance of both process and observation noise can be assumed constant. The second set of experiments consists in printing a stack of leaves using the filtering algorithm for which the obtained results are presented. These results are compared to the ones obtained with two different baselines. The first baseline consists in printing the stack of leaves without any feedback control (open-loop). In that case all leaves have the density that is determined before printing and no measurement is performed during the printing process. For the second baseline, no filtering is used (closed-loop without filtering). The stiffness used to determine the next density input at each step is the value of the measurement at that step. This is equivalent to considering that there is no observation noise.

1.5.1 Determination of the process and observation noises

To evaluate the parameters of the process noise and of the observation noise. A set of 15 single leaves with 5 different input densities was printed. A three-point bending test was performed on each of them and a dataset of loads vs. deflection was acquired. Using a linear regression, the stiffness measured stiffness was obtained. 5 set measurements per leaf were performed Results are presented in Tables A.1, A.2, A.3 of the appendix, and final stiffnesses are showed in Figure 1.13. A first-order regression was then performed between the measured stiffnesses and the infill densities to obtain the values of α and β. The process noise was determined by taking the standard deviation of the means of the measurements per specimen, whereas the observation noise was determined by taking the mean of the standard deviations of the measurements per specimen. With these results the following parameterizations for the process and observation noises are found:

$$\mu_p(d) = 0.3073d + 4.5593 \text{ kg/mm} \tag{1.10}$$

$$\sigma_p = 1.0579 \text{ kg/mm}$$

$$\sigma_o = 0.6907 \text{ kg/mm}$$

1.5.2 Printing the leaf spring

Leaf springs were printed for different values of n and K under the three previously described methods. The two combinations tried for the pair (n, K) are $(3, 30)$ and $(3, 40)$. When performing stiffness measurements, the mean of 5 subsequent measurements was taken. The results of the stiffness measurements are reported in Table 1.1, Figure 1.14, and 1.15. As shown in these figures, the filtering leads to a final stiffness closer to the objective than the baseline methods do.

Consider the case $n = 3, K = 30$ (Figure 1.14), at the first step every process starts with the specimen of the same density, which is the best value according to the prior knowledge.

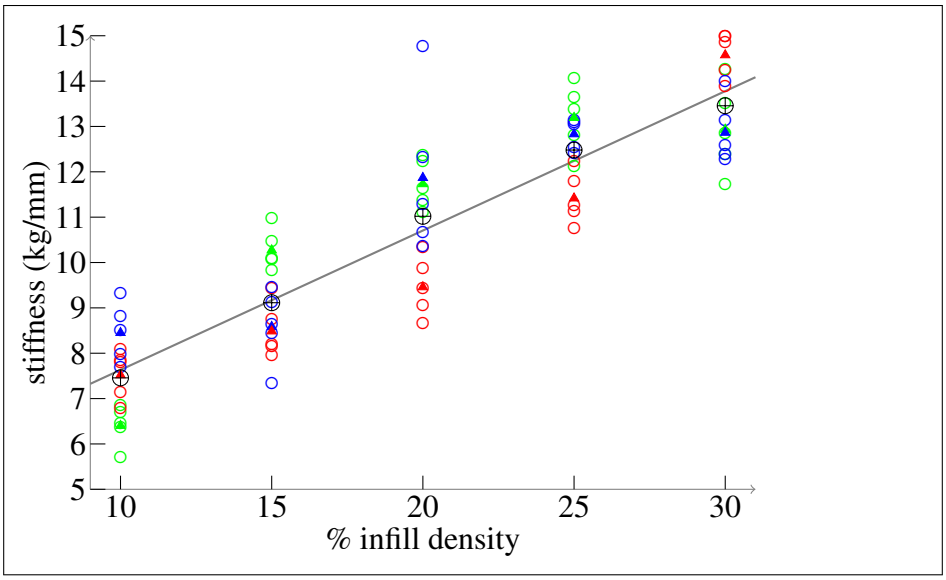

Figure 1.13: Stiffness measurements for 15 specimens of different infill densities. $\circ$ represents each measurement. Δ represents the average stiffness of each specimen from 5 measurements. $\oplus$ represents the average stiffness of specimens with the same infill density. R, G, and B represent the 1^{st}, 2^{nd}, and 3^{rd} specimen of the same infill density, respectively. The line represents the linear regression of $\oplus$ data given by equation (1.10).

Once the measurement has been performed for the closed-loop processes, both of them have the nearly-identical value of stiffness due to the small observation noise. Nevertheless, this value is not exactly the desired one. At the next step, the feedback control corrects that error from the previous step. However, the controller performs better when the stiffness is estimated using the forgoing filter. In the non-filtering case, the stiffness measurement is considered perfect and the information of the control that led to that stiffness is discarded. At the final step, the closed-loop control with filtering reached a better stiffness than both baselines.

Similarly for the case $n = 3, K = 40$ (Figure 1.15), the closed-loop control with filtering provides a better result, even though in the first two steps, the non-filtering controller has its measured values closer to the nominal one.

Whether the poor performance of the open-loop control compared with the closed-loop control is due to a high variance or the process or to a bias in the model is unknown. More experiments would be required to evaluate the actual variance and bias of the open-loop control process. Both probably play a role and lead to complementary conclusions. In the

Table 1.1
Measured stiffness (kg/mm) at steps $1, 2, 3$ using the filtering algorithm and the two baselines with the absolute error in the stiffness at each final step

(n, K)	Closed-loop with filtering			Closed-loop without filtering			Open-loop		
$(3, 30)$	11.53	19.89	**30.43**	11.55	18.65	**29.24**	–	–	**33.49**
Error	1.43 %			2.53 %			11.63 %		
$(3, 40)$	12.53	27.86	**40.89**	12.67	26.31	**42.29**	–	–	**37.09**
Error	2.23 %			5.73 %			7.28 %		

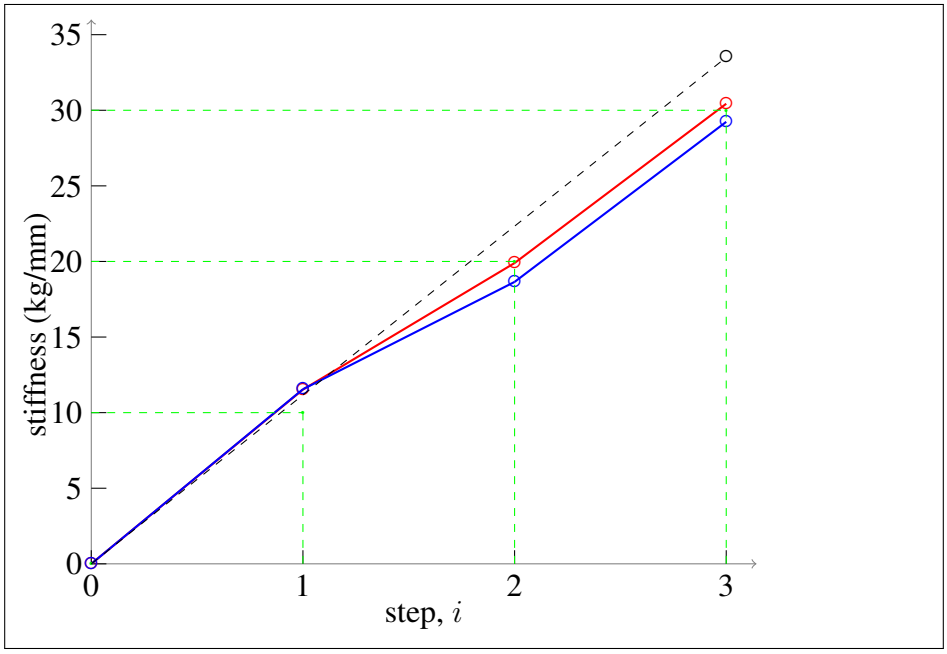

Figure 1.14: Stiffness measurements at steps $1, 2, 3$ for $n = 3, K = 30$. $\circ$ represents a measurement. Red is used for closed-loop with filtering. Blue is used for closed-loop without filtering. Dashed **black** is used for open-loop. Green marked coordinates represent the desired values of stiffness.

case of a high variance, then even an unbiased model could not improve the precision of an open-loop control, thus the relevance of a closed-loop control. However, even if the error of open-loop control is due to a systematic bias in the model used to determine the control, then a better model could potentially yield to results as good or better than the ones obtained here with a closed-loop control. But this actually illustrates the advantage of using a feedback control law: its robustness to model imprecision. Indeed, even with a basic and imprecise model, feedback control can lead to impressively good results as shown in Chapter 2.

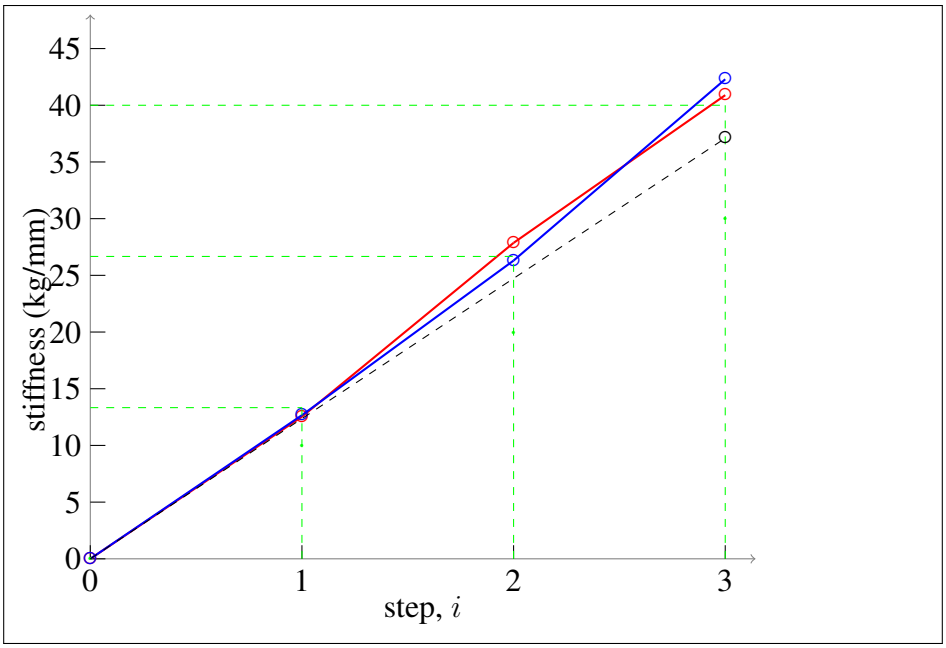

Figure 1.15: Stiffness measurements at steps $1, 2, 3$ for $n = 3$, $K = 40$. Legend is same as in Figure 1.14

1.6 Conclusion

In this chapter, the idea and implementation of a feedback control system for a specific additive manufacturing process are presented. The feedback control is based on measurements taken during the process and aims at reaching a specific desired stiffness for an object comparable to a leaf spring. A better precision was achieved using a closed-loop control with filtering than by using two baselines: a closed-loop control without filtering and an open-loop control. This experiment, while very specific and hardly generalizable as it is, shows the relevance of feedback control in AM. One may argue that what makes this experiment successful is not directly related to the fact that AM is used for manufacturing the final part. But even if a similar experiment could certainly be imagined without using a 3D printer but with another process instead, the material requirements would have been limiting and the whole process more complicated and time-consuming.

CHAPTER 2

A SECOND EXPERIMENT: 3D PRINTING OF A CANTILEVER BEAM

2.1 Introduction

While the experiment of section 1 shows the relevance of feedback control in additive manufacturing, the final object was made of several components printed independently. Moreover, measurements were taken after the completion of each component once it was taken out of the printer, and therefore not directly during the process in the context of an integrated control-observation system. The experiment presented in this section is more sophisticated since a single object is printed with feedback control. Moreover, the manufacturing process is paused after the completion of a given number of layers to take a measurement without moving the partially printed object from the printer. In this experiment, a vertical plastic cantilever beam is printed. The height and thickness of the cantilever have fixed values while the width of the cantilever is variable. The width of the cantilever is progressively modified to control its final stiffness under a single end load horizontal and perpendicular to the axis along which the width is modified.

The control law is based on a model of the cantilever as an Euler-Bernoulli beam whose parameters are determined empirically via some prior measurements.

2.2 Physics

In this section the physical model used in this experiment is detailed. Let x be the horizontal axis along which the stiffness is measured, y the axis along which the width of the beam is adjusted, and z the vertical axis. A load P is applied on top of the cantilever along the x axis. Deflection along axis z is written $v(z)$. The cantilever is made of n stacks of same width layers and each stack has same height h, thickness d and stiffness E. The variable

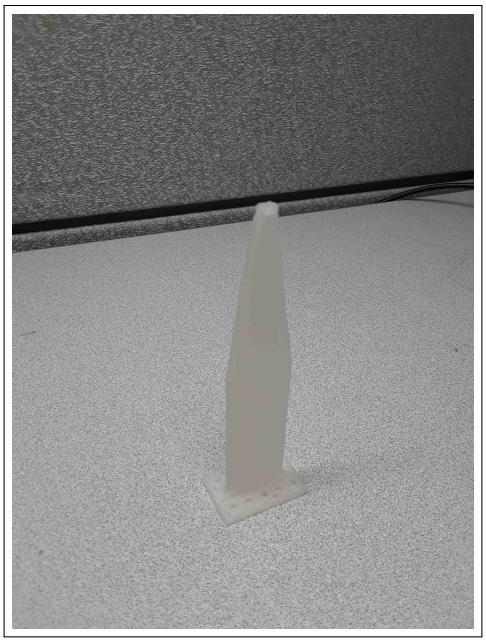

Figure 2.1: Example of a 3D printed cantilever beam

width of a stack of layers is written $w(k)$ for $0 < k \leq n$.

Integrating the Euler-Bernoulli equation yields

$$\frac{\mathrm{d}v}{\mathrm{d}z}(kh) - \frac{\mathrm{d}v}{\mathrm{d}z}(0) = \sum_{j=1}^{k} \frac{12P}{d^3 E w(j)} \left[\frac{h(2nh - (2j-1)h)}{2}\right]$$

$$\frac{\mathrm{d}v}{\mathrm{d}z}(kh + \epsilon h) = \frac{6Ph^2}{d^3} \sum_{j=1}^{k} \frac{2n - 2j + 1}{E(j)w(j)} + \frac{6Ph^2}{d^3} \frac{2(n-k-1)\epsilon + \epsilon^2}{Ew(k+1)}$$

Integrating a second time gives

$$v(kh + \epsilon h) - v(kh) = \left[\frac{6Ph^3}{d^3} \sum_{j=1}^{k} \frac{2n - 2j + 1}{Ew(j)}\right] \epsilon + \frac{6Ph^3}{d^3} \frac{(n-k-1)\epsilon^2 + \epsilon^3/3}{Ew(k+1)}$$

$$v((k+1)h) - v(kh) = \frac{6Ph^3}{d^3} \sum_{j=1}^{k} \frac{2n-2j+1}{Ew(j)} + \frac{6Ph^3}{d^3} \frac{(n-k-1)+1/3}{Ew(k+1)}$$

Therefore the inverse stiffness, or compliance, is equal to

$$\begin{aligned} \frac{v(nh)}{P} &= \frac{2h^3}{Ed^3} \sum_{k=0}^{n-1} \left(3 \sum_{j=1}^{k} \frac{2n-2j+1}{w(j)} + \frac{3(n-k-1)+1}{w(k+1)} \right) \\ &= \sum_{k=1}^{n} \frac{c_{n,k}}{w(k)} \end{aligned}$$

with

$$c_{n,k} = \frac{2h^3}{Ed^3}(6(n-k)(n-k+1)+1)$$

2.3 State estimation

2.3.1 Problem dynamics

We consider a process in N time steps, corresponding to the printing of N stacks of layers. The state of the system at a given step is the reciprocals of the widths of the printed stacks, and all non-printed stacks are attributed a value of 0. Unlike the previous experiment, stiffnesses do not add up at each new step so the state can not be reduced to the stiffness of the partially printed part. The whole information of the different widths has to be retained to be predict the final stiffness, therefore the multidimensional state. The control at a given step is the reciprocal of input width for the next layer added to a drift term. Then the state space is $\mathbb{R}^N$ and the control space is $\mathbb{R}$. The process starts at state

$$s_0 = (0, \dots, 0)^T$$

and the discrete dynamics of the problem are

$$s_k = s_{k-1} + e_k u_k + e_k u_k \epsilon_k$$

With

$$u_k = \frac{1}{v_k + \gamma}$$

Here, e_k is the k-th vector of the canonical basis of $\mathbb{R}^N$, v_k is the input width, γ is an unknown term being interpolated later, and ϵ_k is the gaussian process noise of mean 0 and standard deviation σ_p. The presence of a drift term γ and of a multiplicative noise in the dynamics come from practical considerations regarding the printing process, such as the spreading of the deposited material while still hot after extrusion. Both choices are confirmed by measurements.

2.3.2 Observation of the process

At each time step k the following quantity is observed

$$o_k = C_k^T s_k + C_k^T s_k \nu_k$$

Here, ν_k is the Gaussian process noise of mean 0 and standard deviation σ_o, and C_t is the following vector of size N

$$C_k = (c_{k,1}, \ldots, c_{k,k}, 0, \ldots, 0)^T$$

2.3.3 Kalman filter

In order to maintain an estimate of the state of the system throughout time, a Kalman filter whose update rule is given below is used. μ_k is the state estimate at step k. Only the first k coordinates are considered (the subsequent 0 are ignored).

$$
\begin{aligned}
\bar{\mu}_k &= (\mu_{k-1}, u_k)^T \\
\bar{\Sigma}_k &= \begin{bmatrix} \Sigma_{k-1} & 0 \\ 0 & u_k^2 \sigma_p^2 \end{bmatrix} \\
\Sigma_k &= \left(\bar{\Sigma}_k^{-1} + \frac{C_k C_k^T}{(o_k \sigma_o)^2} \right)^{-1} \\
\mu_k &= \Sigma_k \left(\bar{\Sigma}_k^{-1} \bar{\mu}_k + \frac{o_k}{(o_k \sigma_o)^2} C_k \right)
\end{aligned}
$$

2.4 Control law

In this section, several costs are defined and the corresponding controls are given.

2.4.1 Minimizing the quantity of used material

Let $(u_1, \ldots, u_N)$ be the chosen controls for the whole process, equivalent to the following control widths: $V = (v_1, \ldots, v_N)$ that yield the actual widths $W = (w_1, \ldots, w_N)$. Minimizing the expected quantity of used material is equivalent to minimizing the following sum:

$$\sum_{k=1}^{N} v_k$$

With the objective constraint:

$$\sum_{k=1}^{N} \frac{c_{N,k}}{v_k + \gamma} = \mathcal{C} \tag{2.1}$$

The Lagrangian associated to this problem is:

$$\mathcal{L} = \sum_{k=1}^{N} v_k + \lambda \left[\sum_{k=1}^{N} \frac{c_{N,k}}{v_k + \gamma} - \mathcal{C} \right] + \sum_{k=1}^{N} \mu_k (v_k - v_f)$$

And its partial derivative with respect to v_k is

$$\partial_{v_k}\mathcal{L} = 1 + \mu_k - \lambda\frac{c_{N,k}}{(v_k+\gamma)^2}$$

Setting all these partial derivatives equal to 0 yields

$$v_k = \sqrt{\lambda c_{N,k}} - \gamma$$

λ is found by replacing v_k in the equality constraint 2.1. Therefore

$$v_k = \frac{1}{\mathcal{C}}\left[\sum_{n=1}^{N}\sqrt{c_{N,n}}\right]\sqrt{c_{N,k}} - \gamma$$

Which will be the optimal control at step 1. This is easily adapted to a further time step n by replacing the first $n-1$ v_k by the variables estimated with the Kalman filter and grouping them with the objective $\mathcal{C}$.

2.4.2 Minimizing the probability of failure

A problem that can arise during the 3D printing of several layers is that the printed layer collapses when trying to print a overhang. There is usually a limit overhang angle beyond which printing will not be possible. We can formulate this constraint in the case of the cantilever beam by requiring that when printing a new stack, its width cannot exceed the previous stack width plus a term c depending on the overhang limit angle. With N steps, this constraint yields the following $N-1$ inequalities for $1 \leq k \leq N-1$:

$$w_k + c \geq w_{k+1}$$

Here, the w_k are the actual widths after applying the control width v_k and adding the drift term γ and a noise term of variance σ. Adding a minimum and maximum values for the

widths of the layers yields two new constraints

$$a \geq w_1$$

$$w_n \geq b$$

Let $\mathcal{V}$ be the volume of $\mathbb{R}^n$ defined by these $N+1$ inequalities. The random vector $W = (w_1, \ldots, w_N)^T$ follows the multivariate normal law of mean $V = (v_1 + \gamma, \ldots, v_N + \gamma)$ and covariance σI_N. The probability that W belongs to $\mathcal{V}$ is:

$$P_V = \int_{\mathcal{V}} \frac{1}{\sqrt{(2\pi)^N |(\sigma^2 I_N)|}} \exp\left(-\frac{1}{2}(W-V)^T (\sigma^2 I_N)^{-1} (W-V)\right) dW$$

Taking the gradient of this expression with respect to V gives

$$\begin{aligned}
\nabla_V P_V &= \int_{\mathcal{V}} \frac{1}{\sqrt{(2\pi)^N |(\sigma_p^2 I_N)|}} \exp\left(-\frac{1}{2}(W-V)^T (\sigma_p^2 I_N)^{-1} (W-V)\right) \sigma^{-2}(W-V) dW \\
&= -\int_{\mathcal{V}} \nabla_W \left(\frac{1}{\sqrt{(2\pi)^N |(\sigma^2 I_N)|}} \exp\left(-\frac{1}{2}(W-V)^T (\sigma^2 I_N)^{-1} (W-V)\right) \right) dW
\end{aligned}$$

Let $\mathcal{S}$ be the surface of the simplex $\mathcal{V}$. This surface can be partitioned in $N+1$ surfaces defined by the same inequalities defining $\mathcal{V}$, but by replacing exactly one of these inequalities by an equality. Using the divergence theorem, it can be shown that $\nabla_V P$ is equal to a sum of $N+1$ probabilities of normal over $N-1$ simplexes multiplied by the normal vector of these simplexes. However, these probabilities don't have a closed-form solution, making a minimization problem using the probability of failure (or of violating the constrained) in a combined cost intractable. Therefore, the log-likelihood trick can be used. It consists in considering the log-likelihood of failure instead of the probability directly.

2.4.3 Minimizing the log-likelihood of failure

Letting

$$L_V = \int_{\mathcal{V}} \log\left(\frac{1}{\sqrt{(2\pi)^N|(\sigma^2 I_N)|}}\exp\left(-\frac{1}{2}(W-V)^T(\sigma^2 I_N)^{-1}(W-V)\right)\right)dW$$

The gradient of L_V is given by

$$\begin{aligned}\nabla_V L_V &= \int_{\mathcal{V}} \sigma^{-2}(W-V)dW \\ &= \sigma^{-2}|\mathcal{V}|\,(V^*-V)\end{aligned}$$

Here, V^* is the center of gravity of $\mathcal{V}$.

Therefore, under the objective constraint 2.1, the Lagrangian of the problem is:

$$\mathcal{L} = L_V + \lambda\left[\sum_{k=1}^{N}\frac{c_{N,k}}{v_k} - \mathcal{C}\right]$$

From there, a numerical solver can be used. The exact solution of this optimization problem could also be found by setting partial derivatives of the Lagrangian to 0. This leads to the third-order equation in v_k^2

$$v_k^3 - v_k^* v_k^2 + \lambda\frac{\sigma^2 c_{N,k}}{|\mathcal{V}|} = 0 \tag{2.2}$$

Since

$$\begin{aligned}\mathcal{C} &= \sum_{k=1}^{N}\frac{c_{N,k}}{v_k} \\ &= \frac{|\mathcal{V}|}{\lambda\sigma^2}\sum_{k=1}^{N} v_k(v_k^* - v_k)\end{aligned}$$

$$\lambda = \frac{|\mathcal{V}|}{\mathcal{C}\sigma^2}\sum_{k=1}^{N} v_k(v_k^* - v_k)$$

And the v_k are solutions of the following system of coupled third-order polynomial equations:

$$v_k^3 - v_k^* v_k^2 + \frac{1}{\mathcal{C}} \sum_{i=1}^{N} v_i (v_i^* - v_i) c_{N,k} = 0, \;\; 1 \leq k \leq N \tag{2.3}$$

2.5 Determination of the models parameters

In order to determine the parameters of the model described above, prior experiments were performed on test specimens.

2.5.1 Printed test specimens

Test specimens of fixed heights and thickness and of variable widths were printed previously to attempting any closed-loop control experiment 2.2. The chosen height was 50 mm, the thickness was 3 mm while the different widths were 5, 10, 15 and 20mm. 3 specimens per width were printed for a total of 12 specimens. In this experiment the infill density was constant (30%).

2.5.2 Stiffness measurements

On each test specimen, a stiffness measurement was performed by measuring the force applied on a load cell while deflecting the cantilever beam 2.3. The load was fixed on the 3D printer moving head, and the deflection was controlled by directly moving it with some custom G-code.

5 series of measurements were taken per specimen in order to determine the parameters E, γ, σ_p and σ_o. Load and deflection measurements are shown on Figure 2.4 while Figure 2.5 shows the first-order interpolation between stiffness and width.

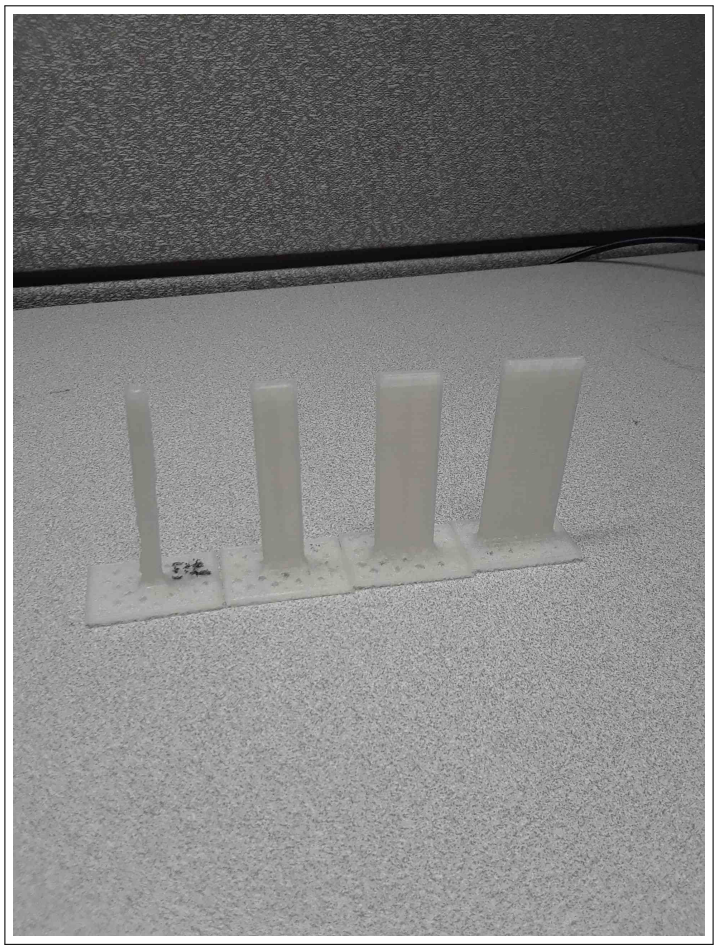

Figure 2.2: 4 specimens of different widths

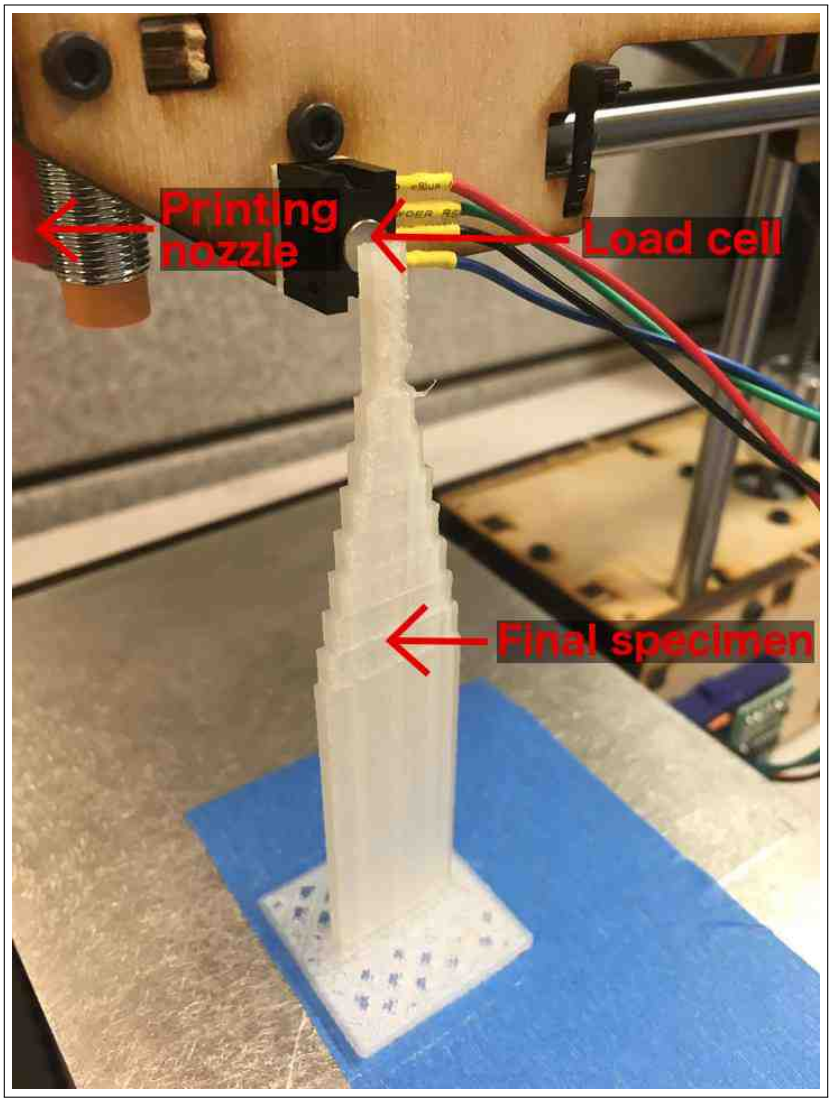

Figure 2.3: Measurement of the stiffness of a full specimen printed with open-loop control

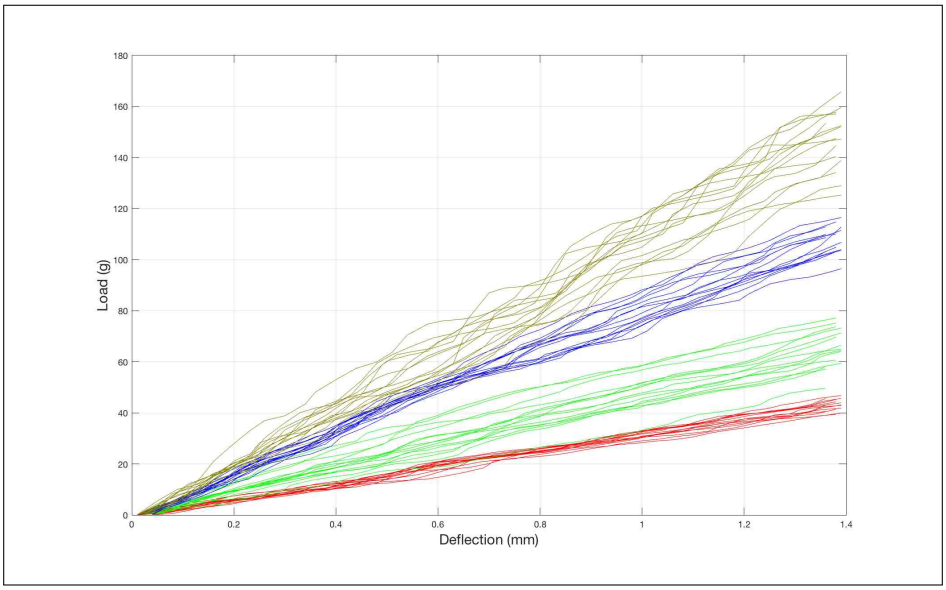

Figure 2.4: Deflection and load measurements on test specimens

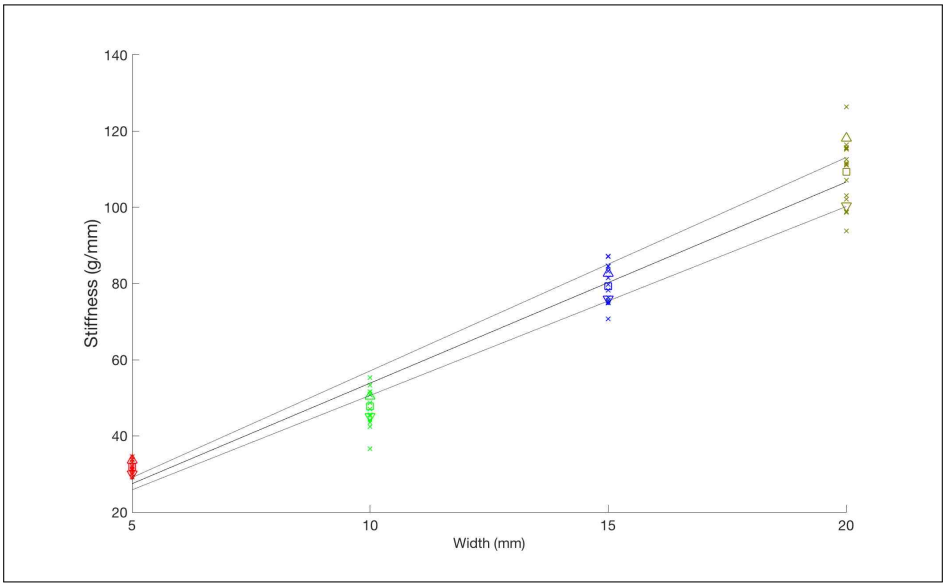

Figure 2.5: Interpolation between stiffness and width of the test specimens

2.6 Experimental results

To assess the performance of the closed-loop controller, a printing experiment was performed based on the cost function minimizing the quantity of used material defined in subsection 2.4.1. The Lagrangian was adjusted by adding a lower and upper bound to the widths of each stack and by enforcing that the successive widths were decreasing. All controls were found using the SLSQP implementation of the SciPy python library.

2.6.1 Experiment description

One specimen was printed with a closed-loop control while three specimens using an open-loop control were printed. Each printed printed had a height of 10 mm, a thickness of 3 mm was made of 1000 layers. For all specimens, the first 500 layers were printed with a fixed width of 20 mm. The 500 remaining layers were partitioned in 10 stacks of 50 layers, each stack having a specific width between 5 and 20 mm. The widths of the 10 printed stacks were predetermined before printing in the case of the open-loop control. When printing with a closed-loop control, a measurement was taken before printing each new stack and the new control determined thereafter. See Table B.1 of the Appendices to see the input controls in the open-loop and closed-loop cases.

2.6.2 Results

After the completion of the printing of each specimen, five stiffness measurements per specimen were taken and compared to the target. Stiffness measurements are reported in Tables B.2 and B.3. The deviation from the compliance target is reported in Table B.4. The deviation for the closed-loop control was 0.16%, whereas the mean of the deviation of the three specimens printed with open-loop control was 22.61%.

2.6.3 Results discussion

There was a significant improvement of the precision of the final compliance of the printed specimen by introducing a closed-loop control. However, the poor results of the open-loop control is mostly due to the simplicity of the model that is used in this experiment. Indeed, the mean and standard deviation of the compliance of the three open-loop specimens are respectively 0.0464 mm/g and 0.004 mm/g while the target was 0.06 mm/g. It means that despite the imprecision of the process giving such a standard deviation, there is also a significant drift not captured in the model that brings the mean so far from the target. But this drift also affects the closed-loop controller since both controllers are based on the same model. Therefore, it shows the whole relevance of using a closed-loop controller: despite an imprecise and somehow poor model, a closed-loop controller can still achieve good results. Now, a legitimate question is to ask if a closed-loop controller would still be pertinent if a sufficiently precise model could predict exactly the expectation of the compliance of a specimen printed in an open-loop fashion. The standard deviation obtained from the three open-loop specimens is an indication that the answer is yes. Assuming that this standard deviation is proportional to the expectation of the compliance, an estimate of the percentage of deviation from the target that would be obtained is the standard deviation divided by the mean of the process. Based on the results of this experiment, this deviation percentage is around 10%, a value still superior to the deviation obtained with the closed-loop control by two orders of magnitude.

2.7 Conclusion

In this chapter, a second feedback control experiment for a specific additive manufacturing process was presented. This experiment aimed at manufacturing a cantilever beam of a specific desired flexural rigidity. In situ stiffness measurements were carried out during the manufacturing process and the closed-loop controller drastically improved the performance

of the final part over the open-loop controller. One of the main conclusions of this experiment is that even with a simple physical model that fails at capturing the whole complexity of the AM process, a feedback control can be robust enough to reach the desired target with a good precision. This is of primary importance since a reason for not using closed-loop control in AM is a difficulty to model the processes involved. The presented results show that this might not be such a problem. To generalize this experiment to different processes and desired object properties, a general framework to describe various object properties and link them to control variables is required. The needs for generalizing this experiment to the printing of arbitrary parts is the subject of the next chapter.

CHAPTER 3
GENERALIZING CLOSED-LOOP CONTROL CAPABILITIES TO THE MANUFACTURING OF ANY PART

In this chapter, the requirements for the generalization of feedback control in additive manufacturing are explored. Three main points, linked to the formulation and solving of a general control problem, are discussed. The first one is the formal description of the problem in term of state, control, cost and objective. The second is, given a formal description of a state, the estimation of its parameters. The third and last point is a description of the available control variables in the case of additive manufacturing. Additive manufacturing encompasses a wide range of fundamentally different processes, based on different materials (like metals and plastics), and that often have several patented variants known under different names. Moreover, while open-source printers become more widespread, especially among hobbyists, most printers are based on proprietary software, making it almost impossible to modify the control algorithms used for the manufacturing of an object. Therefore, creating a global framework for feedback control in AM can sound like a daunting task. But rather than aiming at deriving general control laws which would apply to any object manufactured with any technology, the objective of this work is to pave the way for the creation of a framework allowing to describe all the information necessary for the use of different and unspecified feedback control laws when manufacturing any object with an arbitrary printing process. For that, such a global framework should apply and formulate this information at the level of the 3D printing file. Indeed, despite the multitude of additive manufacturing technologies, all of them rely on a very restricted number of file formats for describing an object to be built. These files are then transformed to a series of computer numerical control instructions that depend on the printer, the software used for generating these instructions and the parameterization of this software for this specific print. There-

fore, the description of an object provided by a 3D printing file is the last representation of an object that all printing processes share in common. For this reason, the position taken in this work is to incite to the creation of systematic rules for including the required information for feedback control in additive manufacturing at the level of the files describing objects that are to be 3D printed.

3.1 Formulation of a general control problem

In order to formulate a control problem, the state space and the control space have to be formulated. However, the space of all manufactured objects, even considering a simple description (like the presence or not of a specified isotropic material at each point of a compact subset of $\mathbb{R}^3$) is infinite-dimensional, and will grow exponentially when adding more properties (anisotropic materials, composite materials, local porosity). To make the problem tractable, a discretization has to be considered, and the level of discretization will depend on the object requirements. The requirements formulated for an object are translated in term of a control problem as an objective. This objective is most likely described as a subset of the state space, where an object satisfies the requirements if and only if the final states belongs to that subset. But the objective can also translate as a final cost function, used to directly define the objective subset or to help the control laws to stir the state to the objective subset during the process. The objective of a general control problem is described more specifically in the next subsection.

3.1.1 Objective definition

In order to specify a control problem for the additive manufacturing of an object, an objective is formulated a set of states that are considered acceptable. To ensure that a state is acceptable, the final printed object has to satisfy different properties that are determined during the design of the object as specifications and that illustrate its purpose.

Properties characterizing a 3D printed object

Here, an attempt is given to classify these different properties under general categories.

1. **Geometric properties**: These properties only characterize the geometry of an object and do not depend on the material used. They are usually implicitly conveyed by a basic 3D printing file format such as STL that only described the geometric representation of the object. Examples: Exact shape, volume, diameter, convexity, number of faces.

2. **Physical properties**: They are properties that depend on the material used and that may also be affected by the process used for manufacturing the object. The information given by standard 3D printing files is not sufficient to describe those properties. They can be divided in 2 subcategories:

   Local properties: These properties characterize the local state of a printed object at a given location, independently of the rest of the object. Examples: Density, stiffness, conductivity.

   Global properties: These properties characterize the whole object printed and usually depend on a combination of the local properties of the object and of its geometry. They are the hardest to verify but often the most useful to the manufacturer as they can translate directly a wide range of different specifications. Examples: Mass, stress under a given load, electrical resistance between two specific points, magnetic moment.

Including the target properties in the formulated control problem

Reaching the desired objective properties at the end of a control problem requires to define what is acceptable for the printed object. Therefore, rather than specifying exact values for the properties to be met, a property is considered satisfied when the quantities involved are close enough to a specified value or belong to an interval also specified by the object

specifications. Such specifications are made to ensure that the intersection of all properties define a feasible and reachable dense subset in the state space describing the printed object.

3.1.2 State space of the system

The description of the state of the system can be the source of many difficulties because of the continuous nature of the problem and the high-number of variables describing the microscopic state of the object. Considering that the microscopic state of the object can be described by n real-valued quantities $f_k(x) \in \mathbb{R}$ at each point of the object $x \in \mathbb{R}^3$, then the most accurate and comprehensive description of the global state of the object at time t is

$$\mathcal{S}_t = \{(x, f_1(x), \ldots, f_n(x), x \in V_t)\}$$

Here V_t is the volume of $\mathbb{R}^3$ where material has been deposited at time t.

However, to make the state of the system tractable, a discretization has to be considered. In that case, instead of considering V_t, a discrete subset V_t' of V_t is considered, leading to a finite state $\mathcal{S}_t' \in \mathbb{R}^{(n+3)|V_t'|}$ with $|V_t'|$ being the size of V_t'. The way of choosing the discretization of V_t depends on the properties to be satisfied. The finer the description is, the more accurate will be the estimation of these properties. Usually, a good discretization will match the vertices used in the 3D printed file describing the geometry of the object, and will be appropriate for the use of Finite Element Methods to verify the properties given in the specifications of the object.

3.1.3 Control space of the system

Describing a control space that fits to every additive manufacturing process is not a realistic task. Rather, the control space varies with many different factors like the specific process, the type of printer that is used and maybe the configuration of the printer. Usually it will include different position values (such as the nozzle position for Fused Deposition Modeling), a possible extrusion rate, different temperatures such as the temperature of the bed or

the temperature of the nozzle.

3.1.4 Dynamics of the system

As for the case of the control space of the system, the dynamics of the system will vary from one process or printer to another. What's more, even for a specific setting, deriving meaningful dynamics from a physics-based model is an extremely complicated task given the complexity of AM processes, and an active area of research [40, 52, 54]. But the relationships between the control variables and the material properties must be known to predict the behavior of a part and adapt the input controls during the process. A modeling step with a physics model can be considered to predict the behavior of the 3D printer in the actual environment of the manufacturing process. [8, 17, 36, 72] give several models especially concerned with thermal processes during specific additive manufacturing. Such models can be used during the feedback control, parametrized and given more or less confidence when performing an estimate of the state of a manufactured build. Examples of modeled properties of the material are its microstructure and the presence of anisotropic tensiles. Because of the layer-by-layer deposition, AM methods create by nature anisotropies in the printed material [27]. These anisotropic properties have been studied for different types of materials, such as the polymer ABS [1] or the Ti-6Al-4V titanium alloy [5, 14]. Both materials are frequently used in AM, and the latter is particularly relevant since it is one of the most common alloys in aerospace industry, a sector directly concerned by low-volume production, and is widely used for biomedical applications like implants and prostheses, two kinds of devices that benefit from efficient mass-customization processes. Moreover, 3D manufactured builds often suffer from end product surface roughness, and their micro structural characteristics are strongly affected by their thermal history, especially for processes like Laser-based additive manufacturing (LBAM), during which a printed build is subject to high temperature gradients and important heating and cooling rates influence the microstructure of the material [2, 8, 9, 29, 32, 41, 64, 71, 82]. Thermal history is also

known to create micro-hardnesses [17, 22, 32, 47, 64] and residual stress [44, 58, 64] in the printed build, degrading it's performance. Modeling those phenomena is a necessary step to achieve the desired optimized topology. Since the goal is this work is to foster the development of closed-loop control for AM processes in general, the details of modeling the dynamics of specific processes are not explored. However, the used dynamics do not especially have to be provided entirely by physical models. They also can be determined empirically via previous measurements on test objects, as done in the experiments of chapters 1 and 2.

3.2 State estimation and process monitoring

One of the main issues of controlling a printing process with a closed-loop is to be able to estimate the state of the printed object during the process. This requires non-destructive methods to evaluate and predict its overall performance. This evaluation is a complex blend of inter-related parameters such as microstructure, density, electronic conductivity, geometry, void density, inter-layer adhesion, elastic modulus shear modulus, and anisotropy. Many of these relationships are inter-related, print-process dependent, and still unknown to the materials science community. For this reason, as for determining the dynamics of an AM process, this work does not pretend to give a systematic way to estimate the state of a printed object during its manufacturing. However, a quick overview of the available methods with some suggestions to link measurements and state estimation are given.

3.2.1 Nondestructive testing

Because the whole purpose of using feedback control laws in AM is to succeed in printing an object conform to the given requirements at first try, every method of testing performed during the manufacturing process has to be nondestructive. Several Nondestructive Testing (NDM) methods exist [7, 15, 33, 57, 61, 69] and The American Society for Nondestructive Testing lists the six following as the most frequently used:

- Magnetic Particle Testing [50]
- Liquid Penetrant Testing [49]
- Radiographic Testing [34]
- Ultrasonic Testing [7]
- Electromagnetic Testing [6, 28]
- Visual Testing

Magnetic Particle Testing and Liquid Penetrant Testing are not suited to AM because of the need to use a foreign material that may interfere with the printing process. However, the other methods can be used to monitor a manufacturing process. Visual Testing can be done via computer vision algorithms to produce a feedback control as done in [67] or [62]. Other NDT methods that can be considered in AM are Laser Testing Methods [42] or Thermal/Infrared Testing [45]. That last method is particularly relevant, since in many processes, the evolution of the temperatures profile of an object being printed has a direct impact on the structural property of the final object once it has cooled down. [23] is an overview of monitoring methods that are compatible with AM processes while [63] studies the materials qualifications for AM using NDT methods.

3.2.2 Relations between NDT measurements and manufactured object state

In order to be able to incorporate the local parameters of the material of what is printed to the state of the system, one must be able to evaluate these parameters with a sufficiently good precision in real-time. With the profile history, thermal history or any other pertinent data of the build that can be measured in real-time, the relevant properties can be reconstituted with various methods. Such methods can be based on a physics model or on data-driven statistical methods.

Physics model based methods

Using physics model to infer the state of an object given observations taken via NDT is a possibility that requires a physics model of the process. As discussed before, this is not the objective of this work and references about modeling specific AM processes can be found in the literature [8, 17, 36, 37, 40, 52, 54, 72]. In [37], a scale measuring the mass of the printed object is used to monitor the manufacturing process, while a thermal camera is used in [32]. [46, 70] give several examples of monitoring processes and ways to correlate raw measurements to mechanical properties.

Data based methods

To derive the state of the printed object given some observations, data based methods relying on machine learning algorithms and statistical models can also be considered [78]. For instance, one can imagine that for a printer using a specific AM process, the following methodology could be used to derive a model: A series of test objects can be printed and monitored using NDT methods, while other measurements, potentially destructive are taken when the object is printed. Those final measurement are used to infer the state of the object and to relate it with the input controls and NDT measurements taken during the process. Therefore, after a sufficient number of test objects has be printed, one can imagine being able to generalize the state inference to other objects using only the NDT measurements and maximum likelihood estimation algorithms like Expectation-Maximization [20].

3.3 Semantic annotations of 3D printing files

Creating a general framework for closed-loop control in AM can only be done by focusing on what all the AM processes have in common. And because additive manufacturing processes differ from one to another in substantive ways, that framework should be independent of the type of AM technology and of the physics involved in the manufacturing

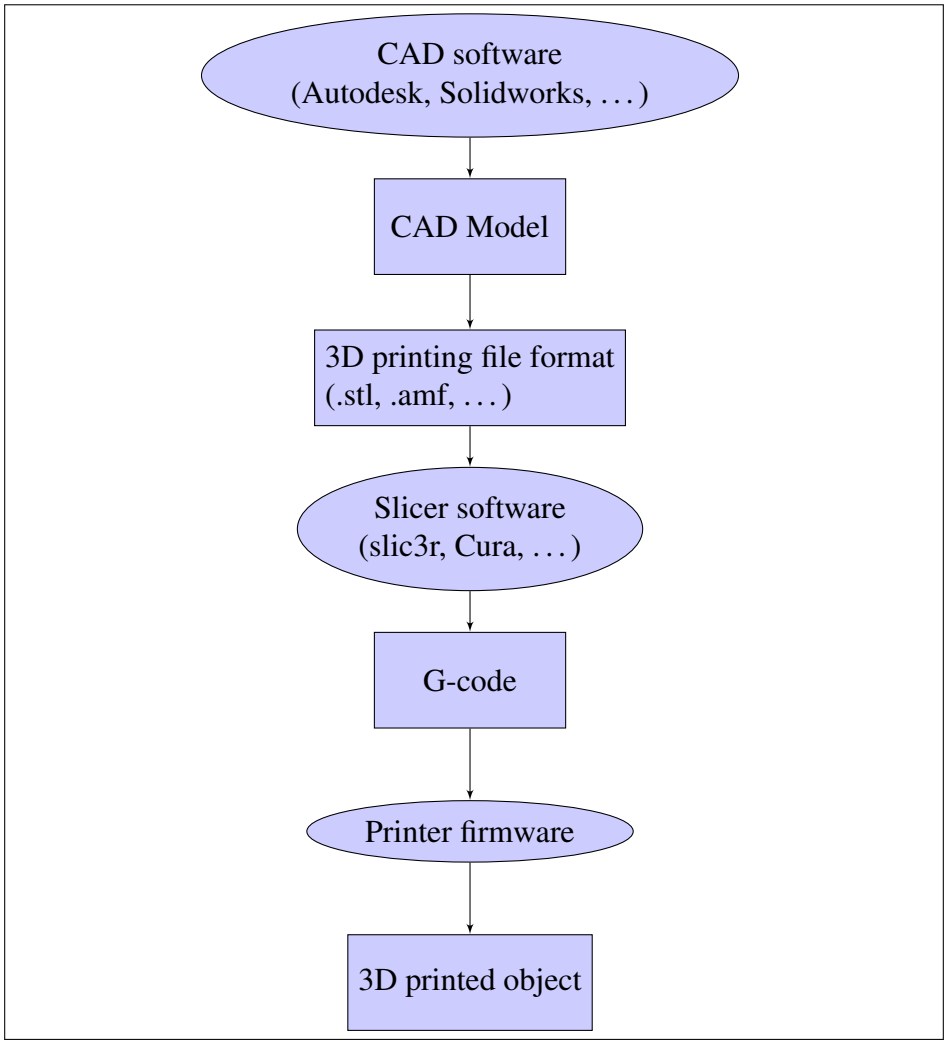

Figure 3.1: Workflow of a typical AM process

process. Looking at figure 3.1, the bottommost element of the diagram common to almost all AM processes is the 3D printing file format. Therefore, this is the reason why this work focus on creating a framework for closed-loop control in AM by suggesting the creation of semantic annotations for 3D printing file format. These rules are meant to provide all the meta-information of an object to be built, including the final desired properties to reach but also the intermediate steps that allow to verify and reach those properties. The idea of semantic annotations comes from the semantics of programming languages. A need exists within the community to develop the semantics of AM print files particularly when compared to the evolution of other sectors such as database management [19], computational finance [83] and reactive software [74]. Only intents to annotate 3D shapes stored in a database through concepts expressed by an ontology were made to ease the retrieval process [4]. Another example of semantic annotations for 3D shapes is in the frame of computer vision to extract relevant object features [43] or represent a robot environment [60]. However, none of these efforts closely relate to the real-time manufacturing context described in this thesis, whose concept is to using formal methods to allow a manufacturing process to evolve on the fly within the specifications of the semantic annotations. In AM, the program is the object to be evaluated, ie. printed. Axiomatic semantics can be used to declare projectively the expected behavior or meaning of that object. This behavior can be all the properties given in the subsection 3.1.1. Therefore, semantic annotations of 3D printing files are a direct way of formulating the objective of the printing process. There is few effort trying to consider the needs in term of digital representation of 3D printing objects for a global improvement of AM processes. The publication [53] suggests an adaption of programming languages tools to improve the quality of the parts built with basic 3D printers, and mentions the possibility of performing feedback control during a process based on video recordings.

```
solid cube
facet normal -0.0 1.0 -0.0
  outer loop
    vertex 0.0 1.0 1.0
    vertex 1.0 1.0 0.0
    vertex 0.0 1.0 0.0
  endloop
endfacet
...
facet normal -1.0 0.0 0.0
  outer loop
    vertex 0.0 1.0 1.0
    vertex 0.0 0.0 0.0
    vertex 0.0 0.0 1.0
  endloop
endfacet
facet normal -1.0 0.0 0.0
  outer loop
    vertex 0.0 0.0 0.0
    vertex 0.0 1.0 1.0
    vertex 0.0 1.0 0.0
  endloop
endfacet
endsolid cube
```

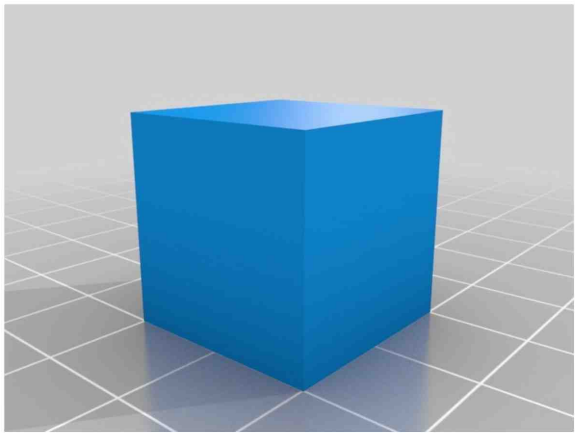

Figure 3.2: Excerpt of an STL file describing a cube

3.3.1 Existing 3D printing file formats

STL

Several file formats exist for additive manufacturing. The most common one is STL (abbreviation of ”stereolithography”) which describe a surface mesh made of triangles (Figure 3.2). STL does not handle multi-material objects does not include any information about the model position, orientation color, texture. Moreover, no mechanism allowing to add comments or meta-information to STL files currently exists. However, STL remains without a doubt the most popular file format for AM.

OBJ

OBJ (abbreviation for ”object”) is the second most popular file format for AM and can handle multiple materials and colors. Another main advantage of OBJ is that it supports both polygonal surfaces and free-form objects. Therefore it can represent complex geometries without relying on approximations by triangles like an STL file would do. OBJ is however a complex format and does not support annotations natively.

AMF

An alternative for AM files is AMF (Additive Manufacturing File Format). It was introduced in 2011 by ASTM International to replace the STL file format. AMF is based on XML and some meta-information can be added to AMF files with the `<metadata>` element tag. AMF can specify several material that can be referenced by volumes or composite materials with proportions which can be position dependent. AMF also has a native support for lattice geometries, include information about scale, orientation, duplicates, colors and textures. This format also support curved triangles, and is then more size-efficient than STL when representing curved surfaces. AMF specifications are defined by an ISO/ASTM standard [39]. AMF should offer enough flexibility to include enough information regarding the properties of the object to be printed in most cases. But a shortcoming of AMF is that its adoption had been slow since it was created, and it might be abandoned as the successor of STL to the benefit of another file format: 3MF.

3MF

3MF (3D Manufacturing Format) is a file format introduced in 2015 by Microsoft to replace STL. It is similar to AMF in term of features and may be more widely adopted because of the participation of important stakeholders of the world of AM in the development of the format. Such as AMF, 3MF is a good candidate for introducing in a file some meta-information that can be used to formulate the objective properties and a closed-loop control problem.

3.3.2 Formal definition of AM files properties

In this section, general guidelines and suggestions about how to define the properties to be verified and how they can be verified. During the manufacturing process, the inversion problem described in Section 3.4, which is performed on the fly, relies on a finite element analysis (FEA) of a volumetric mesh of the build. Even though other analysis methods

can be considered in the long-run, such as multi-physics and multi-scale modeling to accurately understand properties. Finite element methods can solve most nontrivial properties of manufactured objects and can be easily described by the semantic annotations of an AM file. The same way the semantic of programs can help proving them by decomposing an algorithm in small natively provable statements, a volumetric mesh corresponds to a decomposition of a build model that is used to prove relevant complex properties. A volumetric mesh is defined as a set of vertices or nodes with incidence relations that form edges, faces, and elements. The geometry of the mesh specifies the positions of the vertices and other eventual geometric characteristics of the vertices, whereas the topology of the mesh describes the incidence relations between its vertices, edges, faces, and elements. Therefore the metadata included in a particular AM file is supposed to contain the whole information necessary to reconstruct the volumetric mesh used for the FEA. This mesh has been determined prior to the manufacturing in order to provide a sufficient accuracy of the the simulations within a reasonable time. Many techniques exist to generate a volumetric mesh suitable for a FEA from a surface mesh. For instance, TetGen [66], which is a software for tetrahedral mesh generation, can be used to generate a good quality mesh from an AM file. Most of the time, the surface mesh described in an AM file is not directly usable for a FEA since the Delaunay tetrahedralization of its vertices may not even contain all the edges and faces of the surface mesh. In that case a constrained Delaunay tetrahedralization can be performed. A constrained Delaunay tetrahedralization is a tetrahedralization of a set of vertices which contains some predefined edges while being the closest of a Delaunay tetrahedralization of those vertices. See [65] for more details. An example of constrained Delaunay tetrahedralization is given in Figure 3.3.

FEM can provide the approximate solution of a partial differential equation involving two quantities over the domain of the mesh. With FEM, local linear equations approximating the behavior of the object at each node are assembled in a linear equation of the form

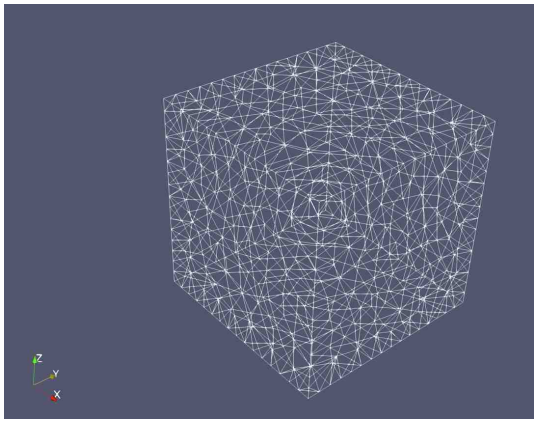

Figure 3.3: Example of a 3D tetrahedral mesh of a cube generated from an STL file with tetgen

$$F = KU \tag{3.1}$$

where F and U are the two vectors representing the quantities of the PDE at each node and K a symmetric positive definite matrix whose coefficients are directly related to the properties of the material at the nodes of the mesh.

Usually, for a specific node, one of the involved quantities is known and the other is unknown. The unknown values are obtained by solving 3.1. Since AM files originally only contain a polygonal surface mesh of the object, the first information to be added to the polygon mesh is the remaining set of vertices used to form a suitable volumetric mesh for a FEA. This would result in a significant but manageable increase of the file size. This volumetric mesh forms the basis for the FEA. Most of the time a Delaunay triangulation of the vertices is sufficient. But it is also possible to consider a different triangulation of the vertices or a tessellation that involves other polyhedra than tetrahedra. In that case the semantic annotations contain the topological information of the mesh (edges, faces, elements).

A volumetric mesh is then obtained on a domain Ω whose boundary $\partial\Omega$ is exactly the surface mesh described by the AM file. To each vertex is added all the necessary metadata to describe the constraints that have to be met and the parameters that are involved in the

verification of those constraints.

Therefore, properties of AM files are not exactly considered, but rather properties of tuples (M, f), where M is a volumetric mesh and f a function which associates to each vertex of M a set of parameters with their respective ranges. Formally, a property is a set of such tuples closed under mesh isomorphism. (M, f) is said to verify the property P if $(M, f) \in P$. For a printed object associated to a volumetric mesh M, the function f is modified during the manufacturing process. Indeed, the vertices belonging to the domain of the object that has already been printed are associated new values with respect to f and the observation of the process. While before printing f associates to vertices expected parameter ranges, it then gives real values or ranges. Even if a printed object can be correctly represented by different couples (M, f) that do not verify the same properties, this problem is not addressed in this work since it is more a question about the reliability of FEM in general, and an accurate mesh is assumed to be chosen.

3.4 From semantic annotations to feedback control laws: Closing the loop based on the represented properties at the file level

Once a correct semantic representation of the expected properties of an object are implemented, along with the methods to prove them with a FEA, control laws specific to AM processes have to be designed. In this section, a way to adapt on-the-fly the local properties of the rest of the build to meet the requirements is suggested.

While the final build is printed, the monitoring of the manufacturing process can evaluate the performance of the build with regard to the semantics of the AM file and what has already been printed. The semantic annotations are used to produce a prediction of the build after termination of the process and to assess if the build specifications are respected or not. If there is a chance that the build will not satisfy the requirements described by the semantic of its file, the printing of the rest of the build can be adapted to meet the final constraints by changing the expected values of the material parameters present in the semantic

annotations, and by changing the control system variables adequately. In most cases, a AM print file and its semantics will exhibit a prescribed geometry constant material properties over the domain of the build. However, the printing process will introduce inherent microscopic defects affecting the material property. With a careful monitoring of these defects and an adapted analysis, if the altered material properties can be estimated on the fly, with micro-mechanical models for example, the control parameters of the printing process can accordingly be modified to obtain different material parameters for the remainder of the build, thus compensating for the initial discrepancy in the expected material properties. In that case, even if the build is designed with already defined constant material properties, the final build is actually printed with varying local properties, optimized during the printing the process. Following the example of the stiffness equation (3.1), adapting the material parameter means determining a new matrix K that contains the information of the known stiffness coefficients k_{ij}^e of the elements of the mesh belonging to the domain of what has already been printed, and that yields a solution to the stiffness equation (3.1) respecting the specifications. Of course, when resolving this problem, the manufacturing constraints must be taken into account too. Whereas in a simulation depending on a stiffness equation such as (3.1), K is usually given and one seeks to find the unique solution of the equation, K is not considered fixed here. The goal of the methods presented here is rather to be able to modify the matrix K, so that the solutions of the stiffness equation are satisfying. This is why this step is later referred as the *inversion problem*.

A way to solve the inversion problem while incorporating all the manufacturing constraints is to perform a multi-scale topology optimization of the rest of the manufactured build to optimize the material properties.

3.4.1 Online topology optimization

Topology optimization is generally adopted to optimize the macroscopic (continuum scale) topology of an object given a set of constraints, loads, and boundary conditions. It is usually

a minimization problem which is solved during the design step of the object with various methods approximating a solution like gradient descent or genetic algorithms. In contrast to traditional approaches to topology optimization, recent work [10] combines topology optimization techniques with advanced microstructural models [11] to optimize the microstructural distribution within a component rather than its macroscopic topology. This multi-scale optimization approach is particularly well suited to 3D printing applications, as this manufacturing process inherently produces microstructures that affect the local material properties of the component, e.g., through the introduction of voids or preferred directions, and hence its performance. One of the main advantages of topology optimization methods is that many various constraints can be expressed in the system to optimize. In the case where the mesh is fixed, the parameters to be optimized are the values of the key parameters at the nodes belonging to the domain of the object that is not yet printed. The same parameters but for the nodes corresponding to the part of the build already printed become fixed values that are involved in the optimization process but not optimized since they cannot be changed anymore. This online topology optimization process allows us to take into account the defects that arise during the manufacturing process and that modify the optimization problem. For the computational efficiency of the online topology optimization, one can imagine methods that do not perform *de novo* the whole minimization step at each step, but reuse the previous results to estimate a new minimum during the manufacturing of the build. For instance, consider a real-valued smooth function F whose domain is an open of $\mathbb{R}_n$, and that represents the function to be optimized with respect to $x \in \mathbb{R}_n$, x being the set of local material parameters that can be controlled. F is assumed to be minimized for $x_0 = (y_0, z_0)$ with y_0 representing the first p coordinates of $x_0, p < n$. The Hessian matrix of F at this point is assumed to be positive definite. The printing process evolves with the objective of reaching x_0, and the first p coordinates of x are now fixed to the value $y_0 + \delta y$ because the printing of the build is not perfectly accurate. Then, instead of recalculating the minimum of $F(y_0 + \delta y, z)$ with respect to z, one can write

$F(y_0 + \delta y, z) = F(y_0 + \delta y, z_0 + \delta z)$ and make a quadratic approximation, assume that $F_{zz}(y_0, z_0)$ is definite positive, such that this quantity can be minimized by taking

$$\delta z = F_{zz}(y_0, z_0)^{-1} F_{yz}(y_0, z_0)\delta y$$

This estimation allows us to save some computational resources, especially since minimization problem can be hard to solve in high-dimensional continuous spaces.

To obtain the desired macroscopic properties, the topology optimization acts on the microscopic parameters that can be modified during the printing process. Those are not always directly controllable but rather influenced by the way the closed-loop control system is parametrized. By modifying the closed-loop control of a 3D printer, the objective is to create specific microstructures to obtain the wanted values for local parameters in the topology optimization. This approach is developed in [10] where a microstructural optimization is performed, enabling the computation of multiscale optimization by tailoring microstructure to obtain desired macroscopic properties. Topology optimization can notably be used to achieve a desired stiffness by minimizing the final weight, for example with Michell structures [48]. [81] studies the topology optimization of structures subject to design-dependent loads while [68] studies tradeoff curves for topology optimization under design constraints. [13, 21, 51, 80] suggest methods more specific to AM that can be adapted for online optimization by manufacturing specific open-cellular structures with pre-selected stiffness.

CHAPTER 4
CONCLUSION

The field of AM is appealing because of the simplicity it offers for manufacturing complex and various parts quickly. And the position taken in this thesis is that it could benefit from the introduction of closed-loop control systems based on widespread methods coming from subfields of optimal control such as stochastic optimal control and filtering. The use of dynamic programming and better control algorithms in general, based on the expected characteristics of an object and nondestructive testing, could leverage the potential of low-cost printers to produce high-quality prints. The first objective of the work presented in this thesis is to show the relevance of closed-loop control in additive manufacturing by presenting two experiments that serve as a proof of concept. Those two experiments proved that by performing intermediate measurements on a partially manufactured object and by relying on dynamics models parameterized by test experiments, one could drastically improve the performance of the printed objects. The second objective is to encourage to the development of a semantic environment for AM files in order to draw a link between the geometrical description of the part, the printing material properties, and the part specifications. Finally, the third is to describe the adaptive mechanisms necessary to modify the local properties of the printed build and to achieve the desired high-level properties. With a semantic environment, a formal description of the part can be provided along with the geometrical description of the part. This environment provides semantic annotations to the volumetric mesh describing the part, so that a topology optimization of the part associated to a closed-loop control is performed during the manufacturing process to thwart the eventual unpredicted printing defects that can arise. This concept can be effective if the AM processes were understood well enough. For many of them, however, this is not currently the case. But even if some AM processes are not understood well enough to be modeled

precisely, some model-free statistical methods can be considered to describe the involved dynamics. What's more, the results of the experiment of Chapter 2 suggest that closed-loop control based on an imprecise model could still be efficient. A significant aspect when performing feedback control in AM is the capability of observing the processes. For that, nondestructive testing technologies such as computed tomography scanning or ultrasonic testing have to be better integrated with 3D printers to perform in situ measurements during printing. Therefore, in a long-term vision, the definition of a formal environment to determine appropriate control laws needs to be general enough to adapt to the progress that can be made in term of AM processes modeling, understanding and sensing. The type of information to be included in semantic annotations for AM print files should then be open to new changes and modifications, and be the result of a common effort between the main actors of the world of additive manufacturing.

Appendices

APPENDIX A

TABLES FOR CHAPTER 1

Table A.1
Mean of the stiffness of each specimen from 5 measurements (kg/mm)

density	1st specimen	2nd specimen	3rd specimen
10%	6.4024	7.5183	8.4502
15%	10.2724	8.4851	8.5846
20%	11.7310	9.4587	11.8682
25%	13.1919	11.4165	12.8316
30%	12.9317	14.5737	12.8644

Table A.2
Standard deviation of the stiffness of each specimen from 5 measurements (kg/mm)

density	1st specimen	2nd specimen	3rd specimen
10%	0.4432	0.5480	0.6473
15%	0.4524	0.5990	0.8108
20%	0.5414	0.6596	1.7784
25%	0.7581	0.5805	0.3430
30%	0.9821	0.5072	0.7098

Table A.3
Mean and standard deviation of the stiffness of specimens of equal density (kg/mm)

density	mean	standard deviation
10%	7.4570	1.0253
15%	9.1140	1.0044
20%	11.0193	1.3533
25%	12.4800	0.9385
30%	13.4566	0.9680

Table A.4
% Printed infill density of the specimen at steps $1, 2, 3$ using the filtering algorithm and the two baselines obtained from equation (1.9)

(n, K)	Closed-loop with filtering			Closed-loop without filtering			Open-loop (at every step)
$(3, 30)$	17.705	15.475	17.375	17.705	15.186	22.108	17.705
$(3, 40)$	28.552	29.648	24.808	28.552	29.634	29.734	28.552

APPENDIX B

TABLES FOR CHAPTER 2

Table B.1
Stiffness measurement at each control step in g/mm (closed-loop) and input width of each stack of 50 layers in mm in the closed-loop and open-loop cases

step	open-loop control	measurement	closed-loop control
1	18.905	86.885	18.930
2	16.908	76.287	16.894
3	14.914	63.049	14.856
4	12.927	52.999	12.813
5	10.932	45.206	10.762
6	8.936	40.367	8.690
7	6.945	36.663	6.551
8	5	28.963	5
9	5	23.222	5
10	5	19.792	5

Table B.2
Stiffness measurements in g/mm of the three completed specimens printed with open-loop control

measurement number	specimen 1	specimen 2	specimen 3
1	19.298	21.220	23.805
2	20.109	20.698	24.284
3	19.738	21.310	25.160
4	20.036	21.223	24.429
5	20.057	19.899	24.294
mean	19.847	20.870	24.394
std	0.340	0.595	0.489

Table B.3
Stiffness measurements in g/mm of the completed specimen printed with closed-loop control

measurement number	measured stiffness
1	15.577
2	17.243
3	16.003
4	17.104
5	17.274
mean	16.640
std	0.793

Table B.4
Percentage of deviation of the final compliance with the target for each specimen

open-loop 1	open-loop 2	open-loop 3	closed-loop
16.02%	20.14%	31.68%	0.16%

BIBLIOGRAPHY

[1] S.-H. Ahn, M. Montero, D. Odell, S. Roundy, and P. K. Wright. Anisotropic material properties of fused deposition modeling ABS. *Rapid prototyping journal*, 8(4):248–257, 2002.

[2] A. A. Antonysamy. Microstructure, texture and mechanical property evolution during additive manufacturing of Ti6Al4V alloy for aerospace applications. 2012.

[3] ASTM D790-17. Standard Test Methods for Flexural Properties of Unreinforced and Reinforced Plastics and Electrical Insulating Materials. Technical report, ASTM International, West Conshohocken, PA, 2017.

[4] M. Attene, F. Robbiano, M. Spagnuolo, and B. Falcidieno. Characterization of 3D shape parts for semantic annotation. *Computer-Aided Design*, 41(10):756–763, 2009.

[5] B. Baufeld, E. Brandl, and O. Van der Biest. Wire based additive layer manufacturing: comparison of microstructure and mechanical properties of Ti–6Al–4V components fabricated by laser-beam deposition and shaped metal deposition. *Journal of Materials Processing Technology*, 211(6):1146–1158, 2011.

[6] Jack Blitz. *Electrical and magnetic methods of non-destructive testing*, volume 3. Springer Science & Business Media, 2012.

[7] Jack Blitz and Geoff Simpson. *Ultrasonic methods of non-destructive testing*, volume 2. Springer Science & Business Media, 1995.

[8] S. Bontha, N. W Klingbeil, P. A Kobryn, and H. L Fraser. Thermal process maps for predicting solidification microstructure in laser fabrication of thin-wall structures. *Journal of Materials Processing Technology*, 178(1):135–142, 2006.

[9] S. Bontha, N. W Klingbeil, P. A Kobryn, and H. L Fraser. Effects of process variables and size-scale on solidification microstructure in beam-based fabrication of bulky 3D structures. *Materials Science and Engineering: A*, 513:311–318, 2009.

[10] Jean-Baptiste Bouquet, Frederic Burgaud, and Julian J Rimoli. Exploiting length-dependent effects for the design of single-material systems with enhanced thermal transport properties. *International Journal of Heat and Mass Transfer*, 101:1227–1236, 2016.

[11] Jean-Baptiste Bouquet and Julian J Rimoli. A length-dependent model for the thermomechanical response of ceramics. *Journal of the Mechanics and Physics of Solids*, 82:82–96, 2015.

[12] D. L Bourell, JJ Beaman, M. C Leu, and D. W Rosen. A brief history of additive manufacturing and the 2009 roadmap for additive manufacturing: looking back and looking ahead. *Proceedings of RapidTech*, pages 24–25, 2009.

[13] D Brackett, I Ashcroft, and R Hague. Topology optimization for additive manufacturing. In *Proceedings of the solid freeform fabrication symposium, Austin, TX*, pages 348–362, 2011.

[14] B. E Carroll, T. A Palmer, and A. M Beese. Anisotropic tensile behavior of Ti–6Al–4V components fabricated with directed energy deposition additive manufacturing. *Acta Materialia*, 87:309–320, 2015.

[15] Louis Cartz. Nondestructive testing. 1995.

[16] Anders Clausen, Niels Aage, and Ole Sigmund. Exploiting additive manufacturing infill in topology optimization for improved buckling load. *Engineering*, 2(2):250–257, 2016.

[17] L Costa, R Vilar, T Reti, and AM Deus. Rapid tooling by laser powder deposition: Process simulation using finite element analysis. *Acta Materialia*, 53(14):3987–3999, 2005.

[18] Dassault Systèmes SOLIDWORKS Corp. SOLIDWORKS Education 2017-2018 edition, http://www.solidworks.com/.

[19] Stefan Decker, Michael Erdmann, Dieter Fensel, and Rudi Studer. *Ontobroker: Ontology Based Access to Distributed and Semi-Structured Information*, pages 351–369. Springer US, Boston, MA, 1999.

[20] Arthur P Dempster, Nan M Laird, and Donald B Rubin. Maximum likelihood from incomplete data via the EM algorithm. *Journal of the royal statistical society. Series B (methodological)*, pages 1–38, 1977.

[21] Z. Doubrovski, J. C Verlinden, and J. MP Geraedts. Optimal design for additive manufacturing: opportunities and challenges. In *ASME 2011 International Design Engineering Technical Conferences and Computers and Information in Engineering Conference*, pages 635–646. American Society of Mechanical Engineers, 2011.

[22] H. El Kadiri, L. Wang, M. F Horstemeyer, R. S Yassar, J. T Berry, S. Felicelli, and P. T Wang. Phase transformations in low-alloy steel laser deposits. *Materials Science and Engineering: A*, 494(1):10–20, 2008.

[23] Sarah K Everton, Matthias Hirsch, Petros Stravroulakis, Richard K Leach, and Adam T Clare. Review of in-situ process monitoring and in-situ metrology for metal additive manufacturing. *Materials & Design*, 95:431–445, 2016.

[24] G. F. Franklin, J. D. Powell, and A. Emami-Naeni. *Feedback Control of Dynamic Systems*. Addison-Wesley, 1986.

[25] W. E Frazier. Metal additive manufacturing: a review. *Journal of Materials Engineering and Performance*, 23(6):1917–1928, 2014.

[26] G-Code. G-code — Wikipedia, the free encyclopedia, https://en.wikipedia.org/wiki/G-code.

[27] W. Gao, Y. Zhang, D. Ramanujan, K. Ramani, Y. Chen, C. B Williams, C. CL Wang, Y. C. Shin, S. Zhang, and P. D. Zavattieri. The status, challenges, and future of additive manufacturing in engineering. *Computer-Aided Design*, 69:65–89, 2015.

[28] Javier García-Martín, Jaime Gómez-Gil, and Ernesto Vázquez-Sánchez. Non-destructive techniques based on eddy current testing. *Sensors*, 11(3):2525–2565, 2011.

[29] SM Gaytan, LE Murr, E Martinez, JL Martinez, BI Machado, DA Ramirez, F Medina, S Collins, and RB Wicker. Comparison of microstructures and mechanical properties for solid and mesh cobalt-base alloy prototypes fabricated by electron beam melting. *Metallurgical and Materials Transactions A*, 41(12):3216–3227, 2010.

[30] JM Gere and SP Timoshenko. Mechanics of materials, 1997. *PWS-KENT Publishing Company, ISBN 0*, 534(92174):4, 1997.

[31] Jim Gill. National MVPA Army Motors edition 92, 2000.

[32] ML Griffith, ME Schlienger, LD Harwell, MS Oliver, MD Baldwin, MT Ensz, M Essien, J Brooks, CV Robino, and JE Smugeresky. Understanding thermal behavior in the LENS process. *Materials & design*, 20(2):107–113, 1999.

[33] Xavier Gros. *NDT data fusion*. Elsevier, 1996.

[34] Randolf Hanke, Theobald Fuchs, and Norman Uhlmann. X-ray based methods for non-destructive testing and material characterization. *Nuclear Instruments and Methods in Physics Research Section A: Accelerators, Spectrometers, Detectors and Associated Equipment*, 591(1):14–18, 2008.

[35] B. Heißing and M. Ersoy. *Chassis Handbook: Fundamentals, Driving Dynamics, Components, Mechatronics, Perspectives*. ATZ/MTZ-Fachbuch. Vieweg+Teubner Verlag, 2010.

[36] D Hu and R Kovacevic. Modelling and measuring the thermal behaviour of the molten pool in closed-loop controlled laser-based additive manufacturing. *Proceedings of The Institution of Mechanical Engineers, Part B: Journal of Engineering Manufacture*, 217(4):441–452, 2003.

[37] D. Hu and R. Kovacevic. Sensing, modeling and control for laser-based additive manufacturing. *International Journal of Machine Tools and Manufacture*, 43(1):51–60, 2003.

[38] Y. Huang, M. C Leu, J. Mazumder, and A. Donmez. Additive manufacturing: current state, future potential, gaps and needs, and recommendations. *Journal of Manufacturing Science and Engineering*, 137(1):014001, 2015.

[39] Standard Specification for Additive Manufacturing File Format (AMF) Version 1.2. Standard, ASTM International, West Conshohocken, PA, 2016, www.astm.org, 2016.

[40] Saad A Khairallah, Andrew T Anderson, Alexander Rubenchik, and Wayne E King. Laser powder-bed fusion additive manufacturing: Physics of complex melt flow and formation mechanisms of pores, spatter, and denudation zones. *Acta Materialia*, 108:36–45, 2016.

[41] PA Kobryn and SL Semiatin. Mechanical properties of laser-deposited Ti-6Al-4V. In *Solid Freeform Fabrication Proceedings*, pages 6–8. Austin, 2001.

[42] AK Kromine, PA Fomitchov, Sridhar Krishnaswamy, and JD Achenbach. Laser ultrasonic detection of surface breaking discontinuities: scanning laser source technique. 2000.

[43] G. Leifman, R. Meir, and A. Tal. Semantic-oriented 3d shape retrieval using relevance feedback. *The Visual Computer*, 21(8-10):865–875, 2005.

[44] F. Liu, X. Lin, G. Yang, M. Song, J. Chen, and W. Huang. Microstructure and residual stress of laser rapid formed inconel 718 nickel-base superalloy. *Optics & laser technology*, 43(1):208–213, 2011.

[45] Xavier PV Maldague. Introduction to NDT by active infrared thermography. *Materials Evaluation*, 60(9):1060–1073, 2002.

[46] M. Mani, B. Lane, A. Donmez, S. Feng, S. Moylan, and R. Fesperman. Measurement science needs for real-time control of additive manufacturing powder bed fusion processes. *National Institute of Standards and Technology, Gaithersburg, MD, Standard No. NISTIR*, 8036, 2015.

[47] J. Mazumder, J. Choi, K. Nagarathnam, J. Koch, and D. Hetzner. The direct metal deposition of H13 tool steel for 3-D components. *JOM*, 49(5):55–60, 1997.

[48] A. George M. Michell. Lviii. the limits of economy of material in frame-structures. *The London, Edinburgh, and Dublin Philosophical Magazine and Journal of Science*, 8(47):589–597, 1904.

[49] Paul E Mix. Liquid Penetrant Tests. *Introduction to Nondestructive Testing: A Training Guide, Second Edition*, pages 221–245.

[50] Paul E Mix. Magnetic particle testing. *Introduction to Nondestructive Testing: A Training Guide, Second Edition*, pages 247–299, 2005.

[51] L. E Murr, S. M Gaytan, D. A Ramirez, E. Martinez, J. Hernandez, K. N Amato, P. W Shindo, F. R Medina, and R. B Wicker. Metal fabrication by additive manufacturing using laser and electron beam melting technologies. *Journal of Materials Science & Technology*, 28(1):1–14, 2012.

[52] Brian N. Turner, Robert Strong, and Scott A. Gold. A review of melt extrusion additive manufacturing processes: I. process design and modeling. *Rapid Prototyping Journal*, 20(3):192–204, 2014.

[53] Chandrakana Nandi, Anat Caspi, Dan Grossman, and Zachary Tatlock. Programming Language Tools and Techniques for 3D Printing. In Benjamin S. Lerner, Rastislav Bodík, and Shriram Krishnamurthi, editors, *2nd Summit on Advances in Programming Languages (SNAPL 2017)*, volume 71 of *Leibniz International Proceedings in Informatics (LIPIcs)*, pages 10:1–10:12, Dagstuhl, Germany, 2017. Schloss Dagstuhl–Leibniz-Zentrum fuer Informatik.

[54] Deepankar Pal, Nachiket Patil, Kai Zeng, and Brent Stucker. An integrated approach to additive manufacturing simulations using physics based, coupled multiscale process modeling. *Journal of Manufacturing Science and Engineering*, 136(6):061022, 2014.

[55] Jayanthi Parthasarathy, Binil Starly, and Shivakumar Raman. A design for the additive manufacture of functionally graded porous structures with tailored mechanical properties for biomedical applications. *Journal of Manufacturing Processes*, 13(2):160–170, 2011.

[56] Printrbot Inc. Simple Maker's Edition (1405) with Rev F Printrboard, https://drive.google.com/drive/u/0/folders/0B9oj0J-4qhdjSUEySGNkTlZzUG8.

[57] Baldev Raj, Tammana Jayakumar, and M Thavasimuthu. *Practical non-destructive testing*. Woodhead Publishing, 2002.

[58] P Rangaswamy, ML Griffith, MB Prime, TM Holden, RB Rogge, JM Edwards, and RJ Sebring. Residual stresses in LENS® components using neutron diffraction and contour method. *Materials Science and Engineering: A*, 399(1):72–83, 2005.

[59] D.A. Roberson, D. Espalin, and R.B. Wicker. 3D printer selection: A decision-making evaluation and ranking model. *Virtual and Physical Prototyping*, 8(3):201–212, sep 2013.

[60] R. B. Rusu. Semantic 3d object maps for everyday manipulation in human living environments. *KI-Künstliche Intelligenz*, 24(4):345–348, 2010.

[61] Ulf Schnars and Rudolf Henrich. Applications of NDT methods on composite structures in aerospace industry. In *Conference on damage in composite materials, Stuttgart, Germany*, pages 1–8, 2006.

[62] Luke Scime and Jack Beuth. Anomaly detection and classification in a laser powder bed additive manufacturing process using a trained computer vision algorithm. *Additive Manufacturing*, 19:114–126, 2018.

[63] Mohsen Seifi, Ayman Salem, Jack Beuth, Ola Harrysson, and John J Lewandowski. Overview of materials qualification needs for metal additive manufacturing. *Jom*, 68(3):747–764, 2016.

[64] N. Shamsaei, A. Yadollahi, L. Bian, and S. M Thompson. An overview of Direct Laser Deposition for additive manufacturing; part ii: Mechanical behavior, process parameter optimization and control. *Additive Manufacturing*, 8:12–35, 2015.

[65] Jonathan Richard Shewchuk. General-dimensional constrained delaunay and constrained regular triangulations, i: Combinatorial properties. *Discrete & Computational Geometry*, 39(1-3):580–637, 2008.

[66] Hang Si and A TetGen. A quality tetrahedral mesh generator and three-dimensional delaunay triangulator. *Weierstrass Institute for Applied Analysis and Stochastic, Berlin, Germany*, 2006.

[67] Pitchaya Sitthi-Amorn, Javier E Ramos, Yuwang Wangy, Joyce Kwan, Justin Lan, Wenshou Wang, and Wojciech Matusik. MultiFab: a machine vision assisted platform for multi-material 3D printing. *ACM Transactions on Graphics (TOG)*, 34(4):129, 2015.

[68] N. Strmberg. An efficient tradeoff approach for topology optimization with manufacturing constraints. In *ASME 2010 International Design Engineering Technical Conferences and Computers and Information in Engineering Conference*, pages 1171–1179. American Society of Mechanical Engineers, 2010.

[69] John Summerscales. *Non-destructive testing of fibre-reinforced plastics composites*, volume 2. Springer Science & Business Media, 1990.

[70] G. Tapia and A. Elwany. A review on process monitoring and control in metal-based additive manufacturing. *Journal of Manufacturing Science and Engineering*, 136(6):060801, 2014.

[71] L. Thijs, F. Verhaeghe, T. Craeghs, J. Van Humbeeck, and J.-P. Kruth. A study of the microstructural evolution during selective laser melting of Ti–6Al–4V. *Acta Materialia*, 58(9):3303–3312, 2010.

[72] E. Toyserkani, A. Khajepour, and S. Corbin. 3-D finite element modeling of laser cladding by powder injection: effects of laser pulse shaping on the process. *Optics and Lasers in Engineering*, 41(6):849–867, 2004.

[73] Ultimaker. CURA 3.1, https://ultimaker.com/en/about-ultimaker.

[74] Timothy Wang, Romain Jobredeaux, Heber Herencia, Pierre-Loic Garoche, Arnaud Dieumegard, Eric Feron, and Marc Pantel. *From Design to Implementation: An Automated, Credible Autocoding Chain fo r Control Systems*, volume 460 of *Lecture Notes in Control and Information Sciences*, pages 137–180. Springer Berlin Heidelberg, 2016.

[75] Jun Wu, Niels Aage, Ruediger Westermann, and Ole Sigmund. Infill Optimization for Additive Manufacturing – Approaching Bone-like Porous Structures, 2016.

[76] J. Xiong and G. Zhang. Adaptive control of deposited height in GMAW-based layer additive manufacturing. *Journal of Materials Processing Technology*, 214(4):962–968, 2014.

[77] Jun Xiong, Ziqiu Yin, and Weihua Zhang. Closed-loop control of variable layer width for thin-walled parts in wire and arc additive manufacturing. *Journal of Materials Processing Technology*, 233:100–106, 2016.

[78] Wentao Yan, Stephen Lin, Orion L Kafka, Yanping Lian, Cheng Yu, Zeliang Liu, Jinhui Yan, Sarah Wolff, Hao Wu, Ebot Ndip-Agbor, et al. Data-driven multi-scale multi-physics models to derive process–structure–property relationships for additive manufacturing. *Computational Mechanics*, pages 1–21, 2018.

[79] Kliment Yanev. Printrun: Pronteface, http://www.pronterface.com/.

[80] P. Zhang, J. Toman, Y. Yu, E. Biyikli, M. Kirca, M. Chmielus, and A. C To. Efficient design-optimization of variable-density hexagonal cellular structure by additive manufacturing: theory and validation. *Journal of Manufacturing Science and Engineering*, 137(2):021004, 2015.

[81] B. Zheng and H. C. Gea. Structural topology optimization under design-dependent loads. In *ASME 2005 International Design Engineering Technical Conferences and Computers and Information in Engineering Conference*, pages 939–945. American Society of Mechanical Engineers, 2005.

[82] B Zheng, Y Zhou, JE Smugeresky, JM Schoenung, and EJ Lavernia. Thermal behavior and microstructural evolution during laser deposition with laser-engineered net shaping: Part I. Numerical calculations. *Metallurgical and materials transactions A*, 39(9):2228–2236, 2008.

[83] Olaf Zimmermann, Sven Milinski, Michael Craes, and Frank Oellermann. Second Generation Web Services-oriented Architecture in Production in the Finance Industry. In *Companion to the 19th Annual ACM SIGPLAN Conference on Object-oriented Programming Systems, Languages, and Applications*, OOPSLA '04, pages 283–289, New York, NY, USA, 2004. ACM.